Continental Shelf Research
April 2020, Volume 195, Pages 104056 (16p.)
https://doi.org/10.1016/j.csr.2020.104056
https://archimer.ifremer.fr/doc/00601/71324/

Phytoplankton distribution from Western to Central English Channel, revealed by automated flow cytometry during the summer-fall transition

Louchart Arnaud [1, *], Lizon Fabrice [1], Lefebvre Alain [2], Didry Morgane [1, 3], Schmitt François G. [1], Artigas Luis Felipe [1, *]

[1] Univ. Littoral Côte D'Opale, Univ. Lille, CNRS, UMR 8187, LOG, Laboratoire D'Océanologie et de Géosciences, F 62930, Wimereux, France
[2] IFREMER, LER/BL, Boulogne sur Mer, France
[3] Aix Marseille Univ., Université de Toulon, CNRS, IRD, MIO, UM110, 13288, Marseille, France

* Corresponding authors : Arnaud Louchart, email address : arnaud.louchart@gmail.fr ; Luis Felipe Artigas, email address : felipe.artigas@univ-littoral.fr

Abstract :

Automated pulse shape-recording flow cytometry was applied to address phytoplankton spatial distribution, at high frequency, in stratified and well mixed water masses in the Western and Central English Channel during the summer-fall transition. Cytometric pulse shapes derived from optical features of single cells allowed the characterization of eight phytoplankton groups. Abundance and total red fluorescence (chlorophyll a autofluorescence) per group were used to define six phytoplankton communities. Their distribution revealed high spatial heterogeneity. Abundance presented a longitudinal gradient for six over the eight groups and succession of brutal shifts along the cruise. Maximum values were often located near the Ushant front in the Western English Channel. A latitudinal gradient characterized the Central English Channel waters under the influence of the Seine estuary. Picophytoplankton (Synechococcus-like cells and picoeukaryotes) represented up to 96% of total abundance and half of the total red fluorescence of the communities near the main front and the Bay of Seine, whereas nanoeukaryotes and microphytoplankton, represented only 4% and less than 1% respectively of total abundance. Both nanoeukaryotes and microphytoplankton dominated the total red fluorescence of the communities of the Central English Channel. The study of traits within each group showed a high variability of traits between communities. The comparison between traits showed that they were independent from each other for some groups (size and red fluorescence per cell for PicoHighFLR and Coccolithophore-like cells; orange and red fluorescence for all the groups), whereas they were dependent for other groups (red fluorescence per cell was dependent of size for picophytoplankton, NanoLowFLR, NanoHighFLR, Cryptophyte-like cells and Microphytoplankton). Variance partitioning revealed that the environmental parameters (temperature, salinity and turbidity) accounted less than spatial descriptors (physical and biological processes) in shaping the communities. Hydrological structures (frontal structures, eddies and tidal streams) were responsible for patches of phytoplankton and defined the structure at the sub-mesoscale (1 – 10 km) in this area.

Highlights

► Automated flow cytometry addresses phytoplankton community changes at high frequency. ► Eight cytometric groups are characterized from pico-to microphytoplankton size range. ► Variation in cytometry-derived traits can be characterized between communities. ► Frontal structures drive phytoplantkon spatial distribution at sub-mesoscale.

Keywords : English Channel, phytoplankton distribution, high resolution, automated flow cytometry, fronts, mesoscale structure

1. Introduction

Carbon uptake and fixation through photosynthesis (Falkowski, 1994; Falkowski et al., 1998; Gregg et al., 2003) make phytoplankton account for up to 50% of the annual global net primary production, while its biomass only represents 2% of the total global biomass (Falkowski et al., 2003; Field et al., 1998). Furthermore, phytoplankton are involved in many biogeochemical cycles (Falkowski, 1994; Falkowski et al., 1998; Gregg et al., 2003) and in most of the marine food webs being a prey for grazers affecting growth, cellular processes and community composition (Holligan and Harbour, 1977; Lampert et al., 1986; Rassoulzadegan et al., 1988). Given the importance of phytoplankton in marine ecosystems, there is a consequent need to perform accurate estimates of abundance and biomass (which are also defined as biological descriptors in the Marine Strategy Framework Directive (MSFD 2008/56/EC) and Water Framework Directive (2000/60/EC) in order to understand the populations assembly into different communities and how these communities influence/determine biogeochemical cycles as well as higher trophic levels (*e.g.* Falkowski et al., 1998; Litchman, 2007; Litchman et al., 2007). The large size-range and diversity of phytoplankton characterise high variations of surface/volume ratios as well as physiological capacities, leading to a different capacity of growth among phytoplankton, sometimes dividing twice a day (Alpine and Cloern, 1988). In addition, environmental drivers are often episodic, contributing to quick changes of phytoplankton responses over space and time scales. Current monitoring sampling strategies might fail to detect these responses (Pearl et al., 2007). Therefore, a trade-off in phytoplankton sampling strategies is needed in order to understand the determinism of phytoplankton changes and distribution, considering both fine space and time scales and environmental parameters.

Considering the techniques available, the use of microscopy and HPLC pigment analysis provide, respectively, high taxonomical and pigmentary composition. However, they are not suitable for high space and time resolution studies (Cullen et al., 1997; Millie et al., 1997; Richardson and Pinckney, 2004) because of the time-consuming and highly specialised work to be carried out back at the laboratory. On the other hand, despite *in vivo* fluorometry could reach a reliable space and time coverage (Rantajärvi et al., 1998), it provides only bulk measurements as estimates of total chlorophyll

a (as a proxy of phytoplankton biomass). Several innovative techniques (*e.g.* multispectral fluorometry, automated flow cytometry, remote sensing) have shown to give representative insights into phytoplankton composition (at least at the functional level), abundance and/or chlorophyll *a* at high resolution (Bonato et al., 2015; De Monte et al., 2013; Lefebvre and Poisson-Caillault, 2019; Marrec et al., 2018, 2014; Thyssen et al., 2015). Among these techniques, automated "pulse shape-recording" flow cytometry (PSFCM) addresses almost the whole phytoplankton size-range (c.a. from less than 1µm to 800 µm width) at single-cell or single-colony level and characterizes them based on their combined or integrated optical properties (*i.e.* light scattering, fluorescence; Dubelaar et al., 2004, 1999). Indeed, this technique records the entire pulse shape of a single particle (Rutten et al., 2005; Thyssen et al., 2008b, 2008a), from small cells as *Prochlorococcus*-like (Marrec et al., 2018) up to large cells and/or colonies of diatoms or *Phaeocystis globosa* (Bonato et al., 2016, 2015; Rutten et al., 2005). Moreover, the cytometric optical properties provide useful proxies of cell length, width, morphology, internal composition and physiology which can be assimilated to functional derived traits. Therefore, the variation of phytoplankton traits at high frequency remain to be investigated across the different spatial scales.

The Western and Central part of the English Channel are well-documented areas which benefit from sustained monitoring (*e.g.* Astan Buoy, Astan & Estacade SOMLIT stations, L4 and E1 stations; Eloire et al., 2010; Goberville et al., 2010; Not et al., 2004; Smyth et al., 2010; Sournia et al., 1987). This epicontinental sea is strongly impacted by climate variability (Goberville et al., 2010) making seasonal and interannual variation in the hydrological and climatic conditions responsible of changes in plankton communities composition (Foulon et al., 2008; Marie et al., 2010; Tarran and Bruun, 2015; Widdicombe et al., 2010). In the Western English Channel (WEC), from May to October, the hydrological conditions go from well-stratified to well-mixed conditions and shape the position of the Ushant tidal front (Pingree and Griffiths, 1978). Eddies that bring high nutrient concentrations in addition to the light, make communities accumulating along the front, especially diatoms and dinoflagellates, and contribute to high biomass (Landeira et al., 2014; Pingree et al., 1979, 1978, 1977). Moreover, the geostrophic flow, eddies, wind upwelling and tidal streams occur along the front

allowing phytoplankton dispersion and crossing the front (Pingree et al., 1979). Therefore, the front extends on scales from meters to kilometres (d'Ovidio et al., 2010; Ribalet et al., 2010). In the Central English Channel (CEC), both the English and the French coast are influenced by river run-off. In the French part, the Seine River contributes to form permanent halocline stratification (Brylinski and Lagadeuc, 1990; Menesguen and Hoch, 1997). During the late summer-fall period, the Bay of Seine is initially characterised by high abundance of diatom (Jouenne et al., 2007). Then, when the depletion of nutrient occurs in summer, diatom abundance decrease and dinoflagellate abundance increase (Thorel et al., 2017). Along the English coast, the Southampton Water estuarine system contributes largely to enhance nutrients along the coast (Hydes and Wright, 1999). Nutrients are especially brought by the Test and Itchen rivers, which drain agricultural land as well as sewage discharge effluents (Hydes and Wright, 1999) resulting in chlorophyll *a* peaks in spring and summer (Iriarte and Purdie, 2004; Kifle and Purdie, 1993; Leakey et al., 1992).

Despite most of phytoplankton studies in the English Channel concerned the coastal areas (*e.g.* Hydes and Wright, 1999; Iriarte and Purdie, 2004; Jouenne et al., 2007; Marie et al., 2010; Not et al., 2004; Pannard et al., 2008; Smyth et al., 2010; Tarran and Bruun, 2015; Widdicombe et al., 2010), some of them concerned coastal-offshore gradients focusing both in the Eastern English Channel (EEC, Bonato et al., 2016, 2015; Lefebvre and Poisson-Caillault, 2019), Central English Channel (WEC, Napoléon et al., 2014, 2012) and Western English Channel (Garcia-Soto and Pingree, 2009; Marrec et al., 2014, 2013; Napoléon et al., 2013) (Garcia-Soto and Pingree, 2009; Marrec et al., 2014, 2013; Napoléon et al., 2014, 2013, 2012). Some attempts were carried out on transects crossing the English Channel in the WEC and CEC (Garcia-Soto and Pingree, 2009; Marrec et al., 2014, 2013; Napoléon et al., 2013). However, these studies reflected three major drawbacks: first of all, some transects were carried out along a latitude gradient, missing the longitude component in which spatial gradients are particularly known to occur in the English Channel (Napoléon et al., 2014, 2013, 2012). Secondly, most of them resulted in a spatial aliasing by missing any fine spatial scale variability. Finally, these spatiotemporal studies mainly sampled the largest organisms (> 20 µm) of the phytoplankton compartment, missing most of the picophytoplankton and the small nanophytoplankton (< 20µm) fraction.

In the present study, we analyse the spatial distribution of some phytoplankton size- and optically-defined functional groups as well as their assembly in communities, highlighting the relation between environmental and spatial features with phytoplankton communities' variability, addressed at high frequency, on a high spatial sampled gridded area. Phytoplankton single-cells and colonies were characterised by continuous recording of sub-surface pumped seawater, by using an automated "pulse shape-recording" flow cytometer coupled to continuous recording hydrological features. With a high resolution spatial sampling strategy, our aims were: (i) to study the phytoplankton distribution per functional group and the variation of the traits within each group across space with respect to meso- to sub-mesoscale hydrological features as frontal areas (ii) to identify the key environmental and spatial variables that could explain the variability between communities' composition and (iii) to define the scale of variability of phytoplankton communities among sites.

2. Materials and methods

2.1 Cruise outlines

Samples were collected during a multidisciplinary cruise focusing on an ecosystemic end-to-end approach of fisheries in the Western English Channel. The CAMANOC (CAmpagne MANche OCcidentale, Travers-Trolet and Verin, 2014) cruise took place on board the RV *Thalassa* (Ifremer) from the 16th of September to the 16th of October 2014, during the summer-fall transition. The ship crossed the English Channel from West to East (Fig. 1). A Pocket-FerryBox system (PFB, 4H-JENA) was coupled to a pulse shape-recording flow cytometer (PSFCM, CytoSense, Cytobuoy), a thermosalinometer (SeaBird SBE21) and an *in vivo* fluorometer (Turner Designs 10-AU). *In vivo* fluorometer required a two steps calibration. The first one used a blank water (de-ionized water) and the second one used a solid standard. The water intake was at the front of the ship's cooling system at a fixed depth (4 m), and in normal ship operation seawater is constantly pumped. The PFB was assembled with sensors for salinity and temperature (Seabird 45 micro TSG), and turbidity (Seapoint). Seawater was pumped at 4 m depth and was continuously analysed by all the sensors. The acquisition of data was continuously performed, and we obtained an integration of the measurement from 1 minute (PFB) to 10 minutes (PSFCM). Because of a relatively brief transit time of water from the water intake to PFB, the observations are representative of sub-surface conditions. The lower resolution was kept to merge phytoplankton functional features with environmental data. The ship navigated at the speed of 11 knots for 1 month. This led to a resolution of approximately 3.4 km (for automated flow cytometry) with a total of 2910 samples, considering stops for discrete fisheries, benthos, plankton and hydrological sampling.

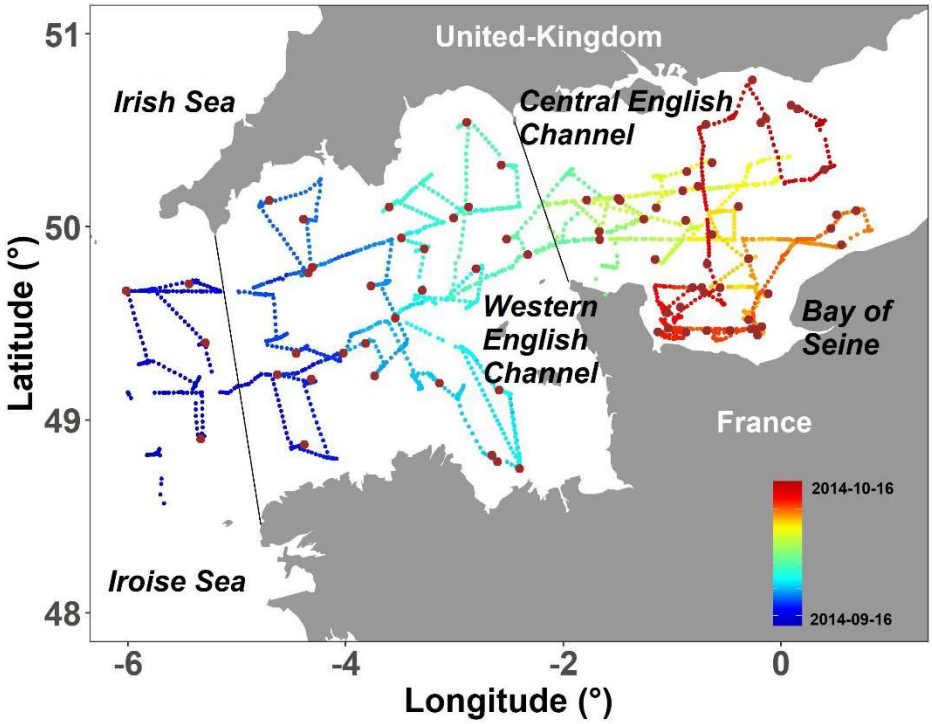

166

167 Figure 1: Continuous recording every 10 minutes by a pulse shape-recording flow cytometer (PSFCM)
168 during the CAMANOC cruise from Sept. 16th (blue dots) to Oct. 16th (red dots) and 78 discrete (CTD)
169 stations (brown dots). Dashed lines correspond to geographical separation of the main regions: Celtic
170 Seas (including Irish and Iroise Sea), Western English Channel and Central English Channel.

171

172 **2.2 Stratification and mixing of water masses**

173 CTD (Seabird SBE 21) casts (78) were performed during the cruise. Temperature (°C), salinity,
174 density (kg.m^{-3}) and depth (m) were recorded at a rate of 1 measure per second. We used the density
175 from the CTD casts to calculate the squared of buoyancy frequency, N^2 (s^{-2}; 3), in order to quantify the
176 vertical density gradient throughout the water column which quantifies the stratification:

177 (3) $N^2 \equiv g/\rho_0 \times (\delta\rho(z) / \delta z)$

178 where g (m.s^{-2}) is the acceleration due to gravity, ρ_0 (1026 kg.m^{-3}) is seawater reference density,
179 $\delta\rho$ (kg.m^{-3}) is the density differential along the water column and δz is the depth of the water column,
180 between surface and bottom.

2.3 Plankton analysis

Continuous pumped waters as well as discrete samples were analysed by a CytoSense (Cytobuoy b.v., Netherlands), an automated flow cytometer (FCM) with the ability of recording the entire optical pulse shape of each particle ("pulse shape-recording flow cytometer": PSFCM). Five signals compose a particle optical profile. The forward scatter (FWS) is collected via a PIN photodiode whereas the sideward scatter (SWS) and three types of fluorescence: red fluorescence (FLR: 668-734 nm), orange fluorescence (FLO: 604-668 nm) and yellow fluorescence (FLY: 536-601 nm) are collected via a photomultiplier. The instrument uses a solid-state laser (Coherent Inc, 488 nm, 50 mV) to analyse, count and characterise single-cells and colonies (Dubelaar et al., 2004; Pomati et al., 2013; Pomati and Nizzetto, 2013) from 1 µm to 800 µm width and a few mm length (Dubelaar et al., 1999). Each particle passes through a 5 µm laser beam at a speed of 2 m s^{-1}. A trigger-level was used on the red fluorescence (FLR) in order to separate phytoplankton and non-fluorescent particles (Thyssen et al., 2015). Continuous recording was performed with this configuration and the trigger-level was set at 15 mV during 9 min at a flow rate of 4.5 µL s^{-1}. The clustering was performed manually with the CytoClus software (Cytobuoy b.v., www.cytobuoy.com). The determination of each group was processed considering the amplitude and the shape of the five signals, referring also to previous work on automated flow cytometry in this area (Bonato et al., 2016, 2015; Thyssen et al., 2015) and according to bead size calibration. In addition, the CytoClus software provides several statistical features on each signal (*e.g.* Length, Total, Average...) as well as the distribution of the different populations of events. The length of the FWS was used as a proxy for cell size. A standardisation of each particle from each cluster was carried out with calibrated beads of 3µm. Two thresholds were set up: the first around 3µm in order to separate picoeukaryotes from nanoeukaryotes and the second around 20 µm in order to separate nanoeukaryotes from microphytoplankton. A group was named according to its estimated size and to its pigmentary features. Following Bonato et al. (2015) particle size was corrected with the measured length FWS of the beads (1 & 2).

(1) Correction factor = real beads size / Measured beads size

(2) Estimated particles size (µm) = Measure particles size × Correction factor

208 Based on the common vocabulary for automated FCM (available at https://www.seadatanet.org), we
209 characterised 6 main functional groups by automated flow cytometry: *Synechococcus*-like cells,
210 picoeukaryotes, nanoeukaryotes, Cryptophyte-like cells, Coccolithophore-like cells and
211 Microphytoplankton. In addition, sub-groups were characterised within the picoeukaryotes and
212 nanoeukaryotes groups, according to their red fluorescence's level. Finally, we defined three
213 picophytoplankton groups (<3µm): *Synechococcus*-like cells, PicoLowFLR, PicoHighFLR; four
214 nanoeukaryotes groups (3 to 20µm): Cryptophyte-like cells, Coccolithophore-like cells, NanoLowFLR
215 and NanoHighFLR; and one microphytoplankton group (>20µm; Fig. 2).

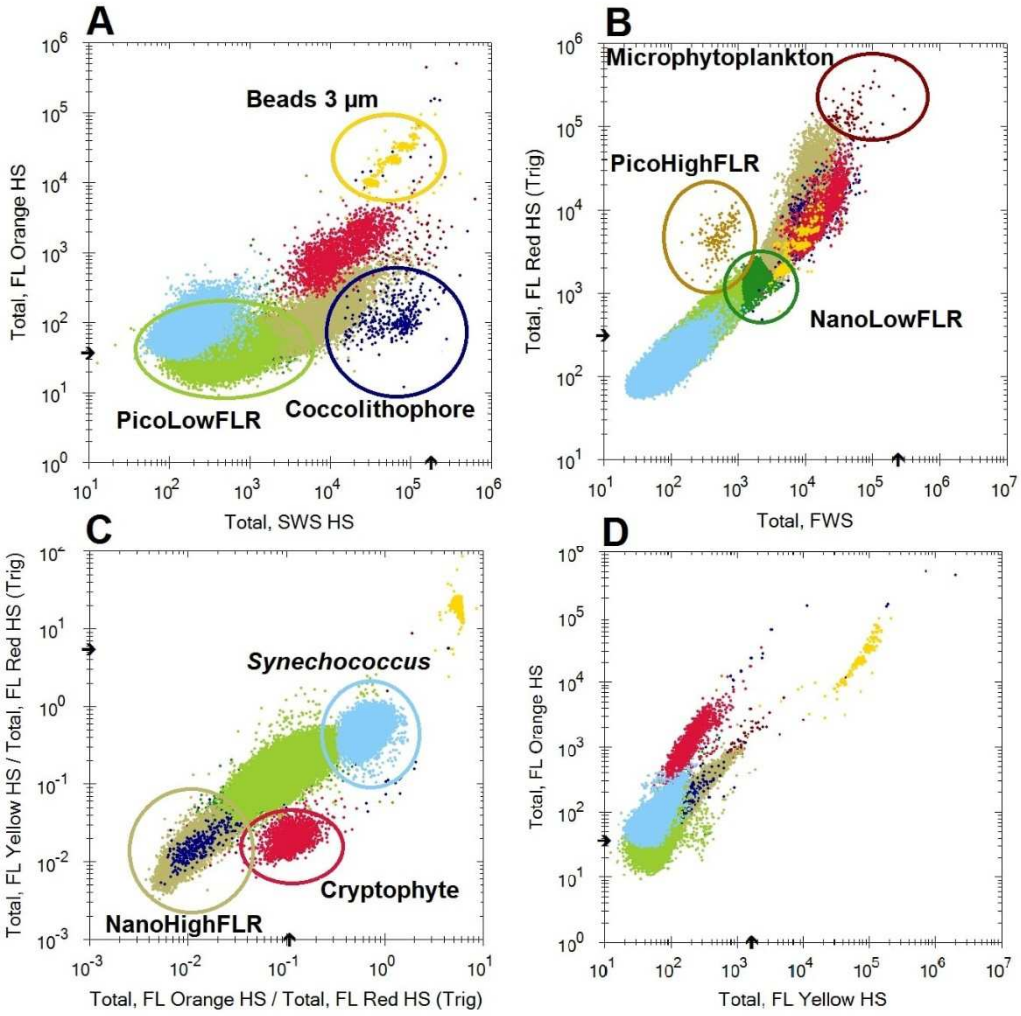

216

217 Figure 2: Cytograms allowing the characterisation of different phytoplankton groups. (A) Total
218 Orange Fluorescence (TFLO) vs. Total Sideward Scatter (Total SWS). (B) Total Red Fluorescence
219 (TFLR) vs. Total Forward Scatter (Total FWS). (C) Ratio of Total Yellow Fluorescence over Total

Red Fluorescence and Total Orange Fluorescence over Total Red Fluorescence (TFLY/TFLR)/(TFLO/TFLR). (D) Total Orange Fluorescence (TFLO) vs. Total Yellow Fluorescence (TFLY). Clusters of single, doubles and triples of beads of 3 µm are merged here.

2.4 Statistical analysis and mapping

We considered the environmental parameters (*i.e.* temperature, salinity and turbidity) and *in vivo* total fluorescence obtained either by the thermo-salinometer (temperature and salinity), the PFB (turbidity) and the Turner fluorometer (*in vivo* total fluorescence) to compute a hierarchical classification analysis based on Euclidean distance. A hierarchical classification was computed also for cytometric groups, separately, to characterize the similarity between the phytoplankton communities among the sites. We used scaled data to detect the similarity among the relative changes in community composition, and we computed the Jaccardized Czekanowski similarity index (also known as quantitative Jaccard). In most recent studies on the spatial distribution of phytoplankton, the common procedure is a computation of Bray-Curtis dissimilarity matrix to define communities (Legendre and Legendre, 1998). However, Bray-Curtis generates a semi-metric matrix which is not as strong as the quantitative Jaccard which generates a metric matrix for cluster analysis. Thus, the Jaccardized Czekanowski index would be more suitable than Bray-Curtis for similarity studies (Schubert and Telcs, 2014). This distance was computed per phytoplankton feature (*i.e.* abundance, red fluorescence) calculated from the cytometric groups such as described in Bonato et al., (2015) in order to get the similarity between pairs of samples. We processed the computation of an average similarity matrix between a matrix based on abundance and a matrix based on red fluorescence. This method is more reliable than using them separately because abundance and red fluorescence (proxy of chlorophyll content which in turn is used as a proxy of biomass) are considered as the main features to discriminate the communities. Each function was weighted between 0 and 1. Abundance accounted for 0.5 as well as red fluorescence. We coupled the final similarity matrix with the Ward method (Ward, 1963) which consist in aggregating at each step the two clusters with the minimum within-cluster inertia and detect the homogeneity of the clusters. Then, the optimal classification cut level was obtained by selecting the maximum average silhouette over the Cophenetic distances. These analyses were processed using

the packages "vegan", "analogue" and "cluster" on R. The importance of environment and space (defined as the Euclidean distance between a pair of latitude and longitude coordinates) for structuring phytoplankton communities was studied among each community by processing a variation partitioning (Borcard et al. 1992, Peres-Neto et al. 2006). In our model, the total variance is represented by four fractions [a + b + c + d] where [a +b] represents the environmental fraction; [b + c] represents the space fraction; [b] is the interaction between environment and space and [d] the residual variance. Space was redefined by the calculation of the principal coordinates of neighbour matrices (PCNM, Borcard and Legendre, 2002) to define them as spatial descriptors of the relationship among sampling units. We used the *pcnm* function from the "vegan" package design for R environment. Phytoplankton communities were detrended using the Hellinger transformation which is appropriate for compositional data by reducing the impact of rare events which are more susceptible to sampling error (Legendre and Gallagher, 2001). In addition, transformation of the data will give the same weight to rare or very abundant groups. Partitions were tested by ANOVA over 999 permutations. Finally, we carried out a multivariate Mantel correlogram to investigate the relationship between geographical distance extracted from the latitude-longitude coordinates and phytoplankton communities over the water bodies. This analysis allowed the detection of the minimal distance at which the correlations disappear.

3. Results

3.1 Hydrobiology

Each continuous-recorded physical variable as well as *in vivo* total fluorescence (µg equivalent of chlorophyll *a* per L) showed a strong spatial structure. The highest salinity values were recorded in the Western English Channel (35.5; WEC) and decreased moderately towards the East (35). In the Central English Channel (CEC) salinity strongly decreased from 35 in offshore waters to 33 in the inner part of the Bay of seine (BOS; Fig. 3A). Colder waters characterised the entrance of the WEC and were surrounded by warmer waters both in the Celtic Seas as well as in mid WEC waters (Fig. 3B). Sharp transitions were evidenced (of only a few kilometres) both at the West and East of the colder area.

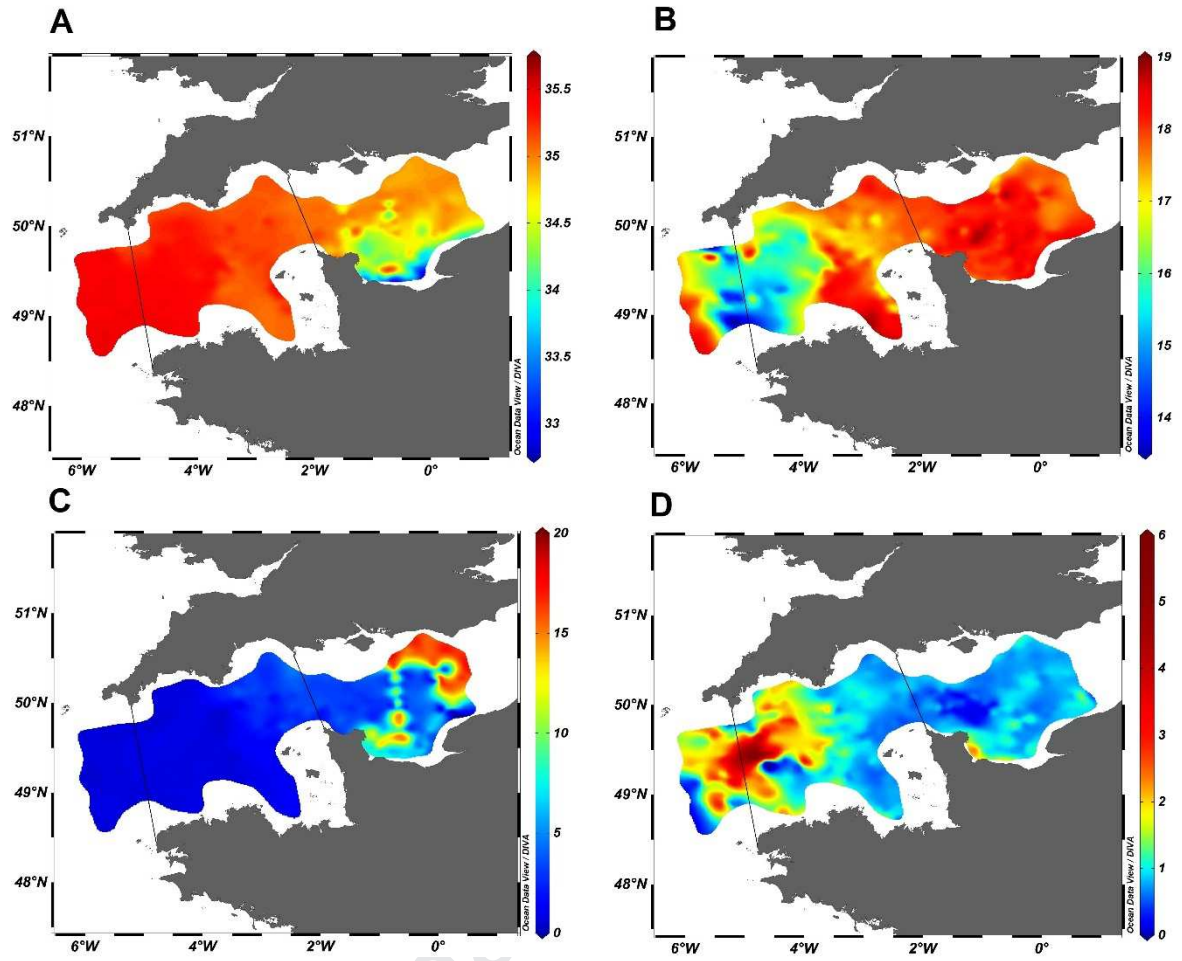

273

274 Figure 3: Continuous recording of: **A.** Salinity, **B.** Temperature (°C) **C.** Turbidity (NTU) **D.**

275 Chlorophyll *in vivo* Fluorescence (µg chl Eq L^{-1}).

The highest turbidity values were recorded in the CEC, both in offshore and coastal waters (Fig. 3C). A sharp increase in chlorophyll *in vivo* fluorescence was evidenced from the outer shelf to the WEC (values shifted from around 0.1 µg chl Eq L^{-1} to 5.7 µg chl Eq L^{-1}). Then, fluorescence levels decreased rapidly eastward in WEC (from 5.7 µg chl Eq L^{-1} to 1-1.5 µg chl Eq L^{-1}; Fig. 3D). Spearman ranks correlation were negative and significant with temperature (ρ = -0.45, $p<0.001$) and turbidity (ρ = -0.29, $p<0.001$) whereas Spearman rank correlation between fluorescence and salinity was positive and significant (ρ = 0.31, $p<0.001$).

Applying hierarchical clustering on the similarity matrix revealed 5 water masses (WM) in the English Channel (Fig. 4A). Mapping these water masses revealed that Western and Central English Channel were structured in hydrological blocks. WM1 corresponded to the eastern part of the Western English Channel and Celtic Seas out of the Channel (Iroise and Irish Seas), whereas WM3 was located in between, in the centre of the WEC. WM2 was located in offshore waters mainly in the CEC. WM4 was under the influence of the Bay of Seine and WM5 was considered as mainly corresponding to the English coastal and offshore waters of the CEC.

Table 1: Minimum and maximum values of temperature, salinity, turbidity and *in vivo* chlorophyll fluorescence (Chl Fluo) among the 5 water masses.

Water mass		Temperature (°C)	Salinity	Turbidity (NTU)	Chl Fluo (µg chl Eq L^{-1})
WM1	Min; max	[16.97; 18.84]	[34.04; 35.49]	[0.01; 3.35]	[0.31; 1.67]
	CV (%)	2.5	0.4	50	25
WM2	Min; max	[17.55; 18.95]	[33.17; 35.16]	[2.62; 4.87]	[0.11; 1.47]
	CV (%)	1.5	1.0	15	39
WM3	Min; max	[13.94; 18.12]	[35.16; 35.53]	[0.51; 1.31]	[0.49; 5.71]
	CV (%)	5.5	0.2	19	48
WM4	Min; max	[17.61; 18.31]	[33.11; 34.82]	[6.23; 14.28]	[0.57; 2.31]
	CV (%)	0.7	1.1	27	33
WM5	Min; max	[16.91; 17.93]	[33.78; 35.00]	[6.34; 18.73]	[0.59; 1.16]
	CV (%)	1.2	0.2	4.5	12

The lowest temperature was recorded in the WM3 revealing also the strongest gradient (ΔT = 4.18°C, Fig.3B and table 1) whereas this water mass exhibited high stable salinity thus the lowest salinity gradient (ΔSAL = 0.37, Fig.3A and table 1) among the water masses. The opposite pattern was observed in the WM1, WM2, WM4 and WM5, the difference of temperature was comprised between

297 0.70°C (WM4) and 1.87°C (WM1) with higher values than in WM3 whereas the salinity difference
298 was comprised between 1.22 (WM5) and 1.99 (WM2) with lower values than in the WM3. Turbidity
299 was also lower in WM3 than in any other WM and showed a small difference (ΔTURB = 0.8 NTU).
300 The highest range of turbidity values were found in the WM4 and WM5 (respectively ΔTURB = 8.05
301 NTU and ΔTURB = 12.39 NTU), both WM under the influence of the Solent (UK) and Seine (France)
302 estuaries. In WM3, *in vivo* chlorophyll fluorescence (Chl Fluo) was higher than in any other water
303 mass and showed the highest variability (ΔChl Fluo = 5.22 µg chl Eq L^{-1}).

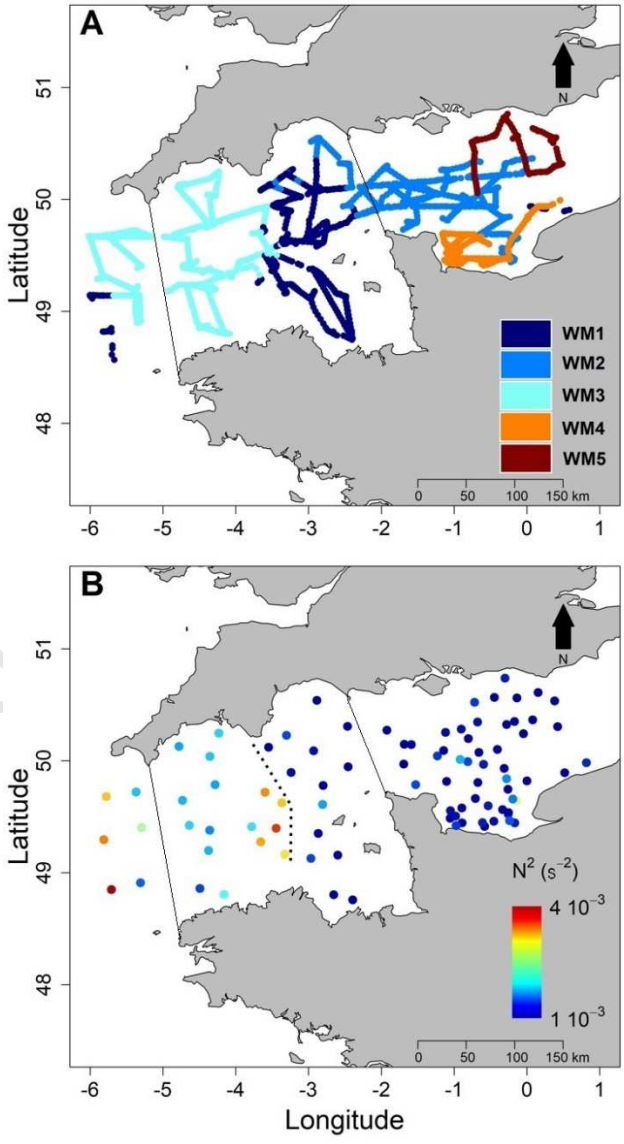

304

305 Figure 4: **A.** Identification of water masses based on results from the Euclidean distance matrix on
306 temperature, salinity, turbidity and *in vivo* chlorophyll fluorescence. **B.** Stratification, value of N^2, as

derived from CTD casts. The dashed line distinguishes homogeneous water masses from heterogeneous water masses and marks the front.

On the West of the main frontal structure (WEC, Fig. 4B), corresponding to WM3, N^2 values were higher and displayed more heterogeneous waters than in the East side (CEC and BOS), where the values of N^2 were lower and displayed homogeneous waters. In the WEC (WM3), N^2 values reached up to 10^{-3} s^{-2} whereas in the CEC and the BOS (WM2, WM4 and WM5), the order of magnitude of N^2 values was between 10^{-4} and 10^{-5} s^{-2} (Fig. 4B). In the Celtic seas, the N^2 was recorded between 3.5 and 4.5 10^{-3} s^{-2} decreasing sharply eastward with the shift of temperature to reach 1.5 10^{-3} s^{-2} in the WEC. They define the outer thermal front as well as the western limit between WM1 and WM3. Then a second change occurred between the WEC and the CEC. The values of the N^2 in WM3 of up to 4.0 10^{-3} s^{-2} shifted to 10^{-4} /10^{-5} s^{-2} the CEC (WM2, WM4) and the BOS (WM5) defining the inner thermal front.

3.2 Phytoplankton abundance, fluorescence and spatial distribution.

Picoeukaryotes (PicoLowFLR and PicoHighFLR) and *Synechococcus*-like cells dominated the phytoplankton abundance. They were structured along a decreasing West-East longitudinal gradient but showing an important heterogeneity in spatial distribution (Fig. 5). High abundance was recorded in the Western English Channel (mostly in WM3) whereas low values were recorded in the Central English Channel and, for Picoeukaryotes, at the western entrance of the English Channel (Celtic Seas, Fig. 5 and 6). However, the abundance of *Synechococcus*-like cells was high out of the Channel and in the WEC, and low in the CEC (Fig. 5A). PicoLowFLR abundance exhibited patches reaching more than 1×10^4 cell mL^{-1} in the WEC (5% of the highest abundance were representing 950 km^2) and close to the Channel isles (Fig. 5B). PicoHighFLR (Fig. 5C) and Cryptophyte-like cells (Fig. 5D) showed the same patterns: low abundance out of the English Channel, sharp increase and high abundance in the WEC (both coastal and offshore waters, WM3), then a sharp decrease and low abundance in the eastern WEC and CEC. Coccolithophore-like cells (Fig. 5E) exhibited high abundance out of the

Channel (western WM1), while the abundance remained low elsewhere. NanoLowFLR (Fig. 5F) showed several patches of high abundance (5% of the highest abundance represented 1000 km^2) between the limits of WM3 (out of the Channel and in the WEC). In the CEC and BOS, the abundance was low. NanoHighFLR high abundance was also detected in WM3, forming a large patch in offshore waters of the WEC (Fig. 5G), decreasing westward and eastward, showing an increase in a restricted area in the Bay of Seine. Microphytoplankton abundance (Fig. 5H) was low out of the English Channel. Then, patches of high abundance were observed in western WM3, in offshore waters of the WEC. In the CEC and BOS, the abundance was low.

The abundance of each group was compared with respect to the distance of the inner WEC thermal tidal front used as an arbitrary geographical reference (Ushant front, Fig. 6). Samples located to the West of the front were represented by a negative distance whereas samples located to the East of the front were represented by a positive distance. A global view revealed that abundance increased as the sample got collected closer to the Ushant frontal area (Fig. 6). This was the case for PicoHighFLR (Fig. 6.C), Cryptophyte-like cells (Fig. 6.E), and NanoLowFLR (Fig. 6.F). On the other hand, NanoHighFLR (Fig. 6.G.) and Microphytoplankton groups (Fig. 6.H.) showed maximum abundance slightly offset (westward) of the front (microphytoplankton also showing high values all along the front). For these groups (PicoHighFLR, Cryptophyte-like cells, NanoLowFLR, NanoHighFLR and Microphytoplankton), the highest levels of abundance were recorded in WM3 which is the most stable water mass observed here. PicoLowFLR (Fig. 6.B), *Synechococcus*-like cells and Coccolithophore-like cells showed a different pattern. The first two groups exhibited high abundance along and across the front in the Western English Channel and in the Celtic Seas (Fig. 6.A) whereas Coccolithophore-like cells showed highest abundance only in shelf waters at the western entrance of English Channel (Fig. 6.D) where waters remained warm and stable (outer front of the WEC). At the East of the inner front, the abundance decreased slowly to reach low values at 100 km from the main frontal system (Fig. 6). At 200 km from the front, a second increase of abundance was observed (Fig. 6) for some groups. A *Synechococcus*-like cells (Fig. 6.A.), PicoLowFLR (Fig. 6.B), PicoHighFLR (Fig. 6.C), NanoHighFLR (Fig. 6.G) and, to a lesser extent, Microphytophytoplankton (Fig. 6.H) and

Coccolithophore-like cells (Fig. 6.D) showed high values compared to the remaining CEC. However, this second peak was 2 to 3 times lower than the one observed close to the main front and could be related to the Seine river plume.

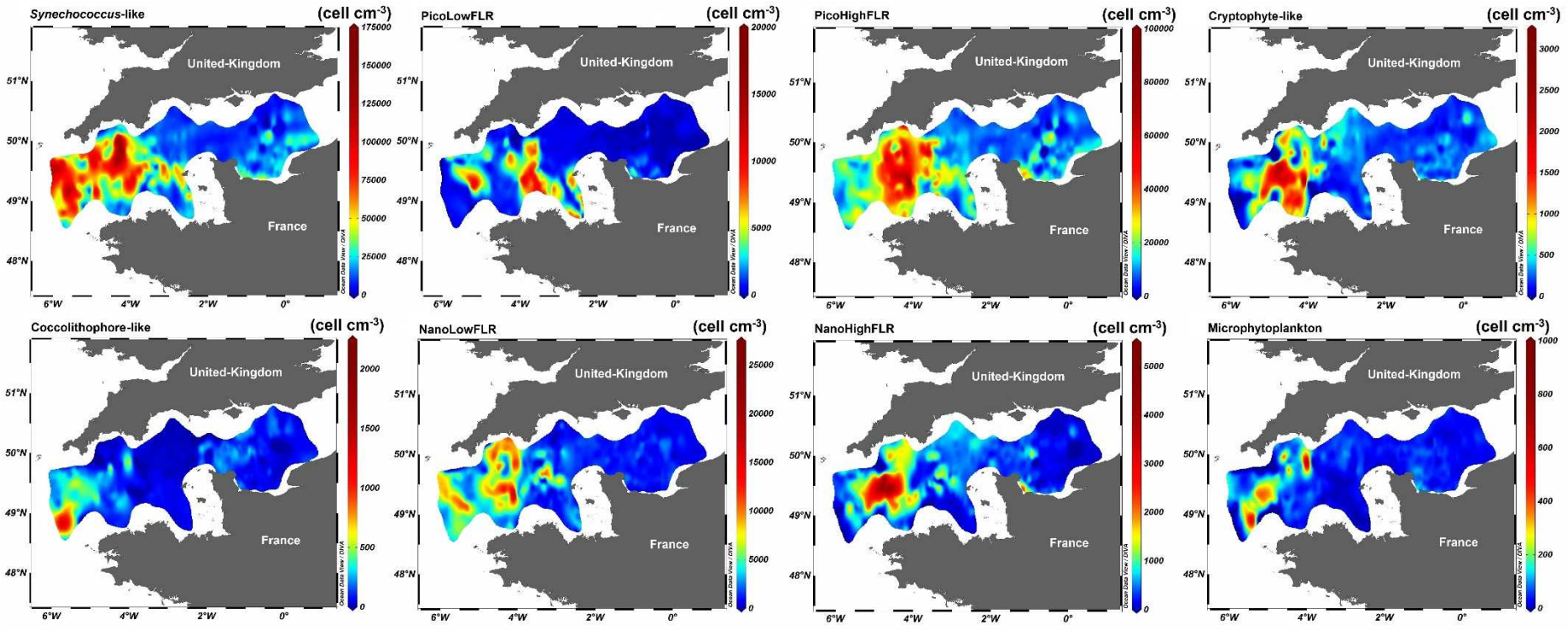

Figure 5: Spatio-temporal distribution of the abundance of the eight phytoplankton groups characterised by the PSFCM.

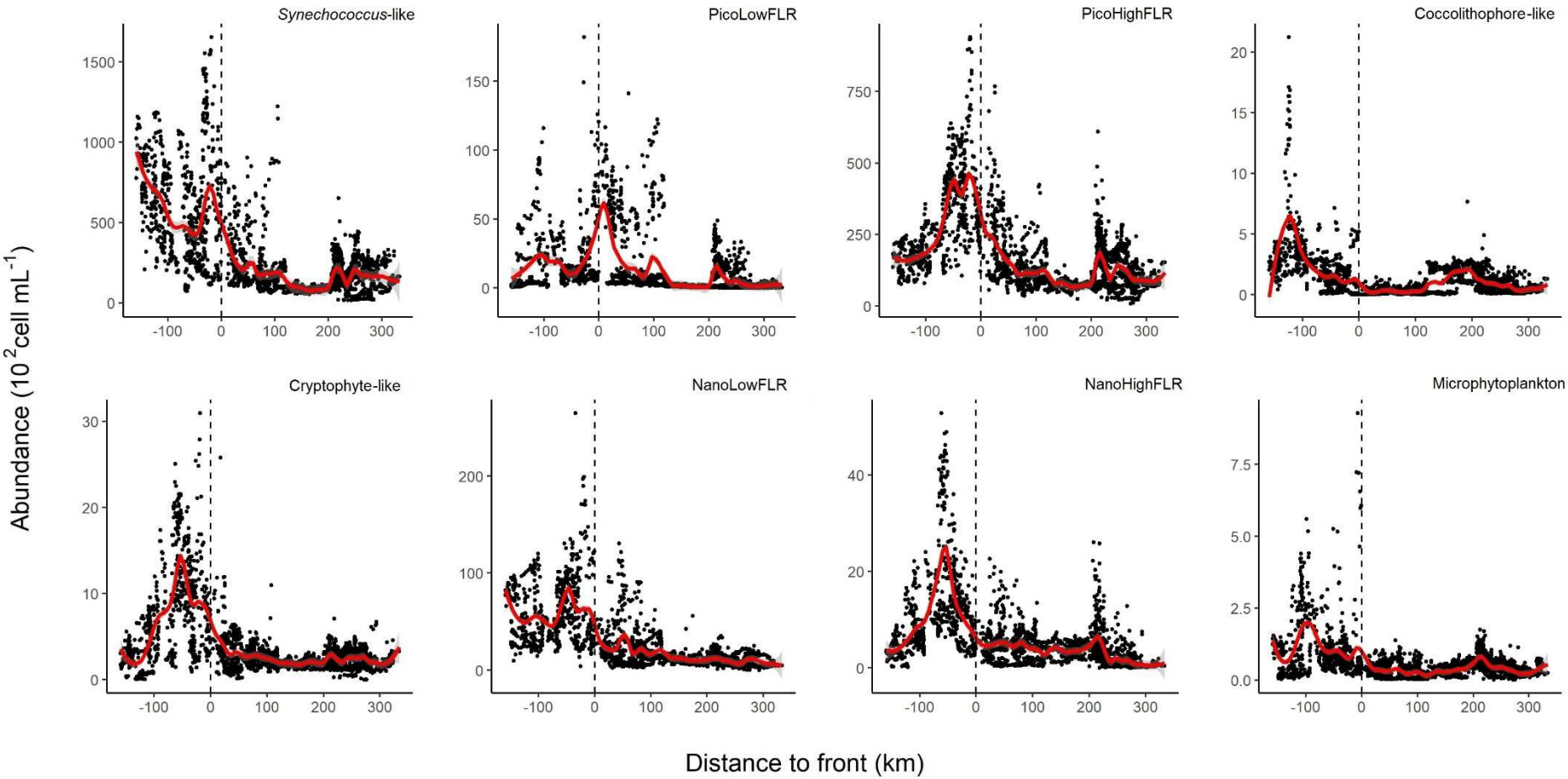
Synechococcus-like
PicoLowFLR
PicoHighFLR
Coccolithophore-like
Cryptophyte-like
NanoLowFLR
NanoHighFLR
Microphytoplankton
Abundance (10 2cell mL -1)
Distance to front (km)

366

367

Figure 6: Distribution of the abundance in relation to the distance to the Ushant front (km) for the eight phytoplankton groups characterised by the CytoSense. The dashed line represents the position of the inner thermal front. Negative distance represents samples at the West of the front. Positive distance represents samples at the East of the front.

3.3 Phytoplankton communities structure analysis.

Phytoplankton communities were discriminated after the computation of a hierarchical classification of the quantitative Jaccard index on abundance and red fluorescence (Fig. 7). The Analysis of Similarity (ANOSIM) provided evidence of a spatial clustering of 6 communities (R = 0.50, *P* = 0.001). However, due to discontinuity between the community C5, we split C5 in C5a and C5b for the investigation of the spatial scale analysis. C1 and C2 were characterised in offshore waters between WEC and CEC (mainly eastern offshore part of WM1 and offshore WM2. C3 was found in the Central English Channel and characterised also the Eastern part of the Bay of Seine (BOS), mainly WM2 and WM5. C4 was located by the inner thermal front (Fig. 4B). C5 community was found in the Western part of the BOS (WM4; C5a) and also in the French part of the WEC (WM3; C5b). C6 corresponded to most of the WEC offshore waters (WM3) including external Channel stations (western part of WM1).

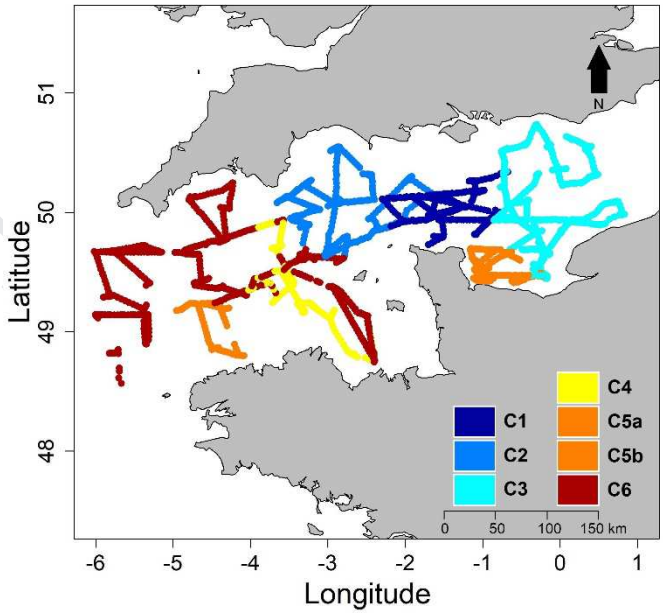

Figure 7: Phytoplankton communities based on the results of the fusion between Jaccard similarity matrice on the abundance and red fluorescence.

Heterogeneity was supported by the values of the coefficient of variance (CV) calculated for each group, in addition, to minimum, maximum of abundance and total red fluorescence (further details in

supplementary table A.1). In terms of abundance (Fig. 8), phytoplankton communities were all dominated by the *Synechococcus*-like group (47% in C5 to 61% in C6 to the total abundance). Picoeukaryotes (*i.e.* PicoLowFLR and PicoHighFLR) groups represented the second most important groups (Fig. 8). However, in C1, C2, C3 and C5, the PicoLowFLR (36% in C3 to 43% in C5) dominated over the PicoHighFLR (1% in C1, C2 and C3 to 3% in C5) whereas in C4 and C6, the PicoHighFLR (24% and 34% respectively in C4 and C6) dominated over the PicoLowFLR (7% and 13% respectively in C6 and C4). On the other hand, the total abundance of nanoeukaryotes was always low (at most they represented 11% of the total abundance for C1). The most abundant nanoeukaryotes group was NanoLowFLR (3% in C3 and C4 to 7% in C1). In C2, the Cryptophyte-like cells total abundance was the double than in any other assemblages. The most important contribution of the Coccolithophore-like cells was found in C1 (1%) whereas in the other communities they accounted for less than 1%. Finally, the total abundance of the microphytoplankton in every community was below 1%.

Although small photoautotrophs significantly dominated abundance (Fig. 8) in both WEC and CEC during the cruise, the contribution of nanoeukaryotes and microphytoplankton to total red fluorescence, which is an estimation of chlorophyll *a* fluorescence (Haraguchi et al., 2017), was important (supplementary table A.1, Fig. 8). The relative contribution of the Coccolithophore-like cells to the total red fluorescence was almost seven times higher in C1 than in any other community. On the other hand, nearly half of the total red fluorescence in C3 and C4 was attributed to *Synechococcus*-like and picoeukaryotes groups (C3: 49% and C4: 50%). This was higher than in the other communities (range between 25% in C6 to 34% in C1 and C2). In C1, C2, C3 and C5, Cryptophyte-like cells total red fluorescence represented the double (12-13%) of what they represented in C4 and C6 (respectively 5% and 6%). In C3, C4 and C6, NanoLowFLR contribution to the total red fluorescence (respectively C3: 17%; C4: 27% and C6: 32%) was higher than the contribution of the NanoHighFLR (C3: 8%; C4: 13% and C6: 29%). We noticed the opposite pattern in C1, C2 and C5. Despite the low abundance of the microphytoplankton group, the contribution to total red fluorescence of this group was comprised between 4% (C4) and 15% (C1).

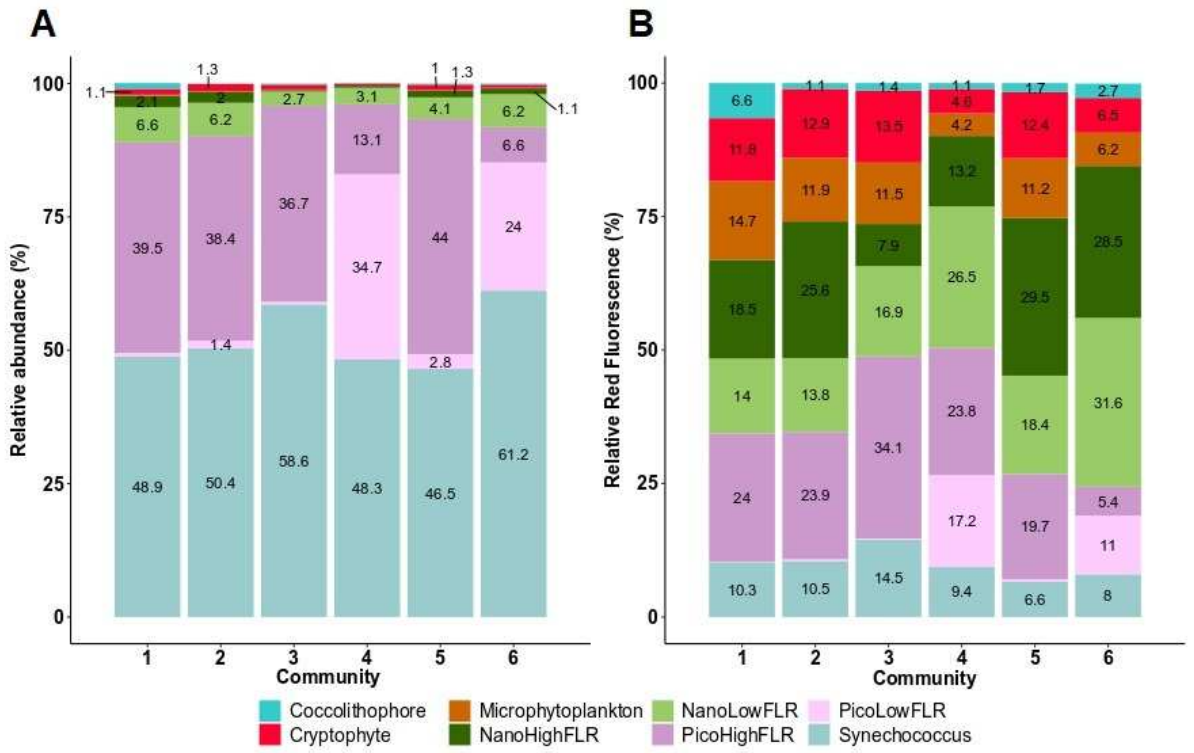

Figure 8: Relative contribution of phytoplankton, A. abundance and B. total red fluorescence, within each community. Only the percentage above 1% are displayed.

Although we observed an heterogeneity in total red fluorescence per cluster, the CytoSense provided us with information on single-cell level features (Fig. 9). Therefore, working at the individual level led us to study the population variability considering a cytometric-derived trait. Here, we first focused on the red fluorescence per cell and then on the cell-size. Different spatial patterns of red fluorescence per cell and cell size were observed, per group, among the communities. *Synechococcus*-like red fluorescence per cell remained unchanged in all the communities despite changes in cell size and abundance (Fig. 9 A and B). Cell size was significantly different between all the communities identified ($p<0.01$). Both picoeukaryote groups (*i.e.* PicoLowFLR and PicoHighFLR) exhibited the most important red fluorescence per cell in C4 and C6 than in the other communities ($p<0.05$). For the PicoLowFLR, the community comparison showed a large range of abundance within an order of magnitude of 10^2 cell mL^{-1} whereas red fluorescence level remained between 200 and 400 a.u. $cell^{-1}$ (Fig. 9A). An increase in the red fluorescence per cell was observed with an increase of the cell size

(Fig. 9B). On the contrary, for the PicoHighFLR, high red fluorescence levels were consistent with low abundance (Fig. 9A) and different relation between red fluorescence and cell size were observed (Fig. 9B). Small cell with high red fluorescence levels were found in C4 and C6. Small cell with low red fluorescence were found in C1, C2 and C4 and large cell with some level of red fluorescence were found in C3. Concerning Cryptophyte-like cells and Microphytoplankton groups, the highest red fluorescence values per cell were found in C5 and C6 and were significant ($p<0.05$). In these communities, the Cryptophyte-like cells exhibited also the highest abundance (Fig. 9A and B) and their cell size was significantly larger in C4, C5 and C6 than in C1, C2 and C3 ($p<0.05$). Coccolithophore-like cells showed higher red fluorescence per cell in C2, C4 and C6 than in C1, C3 and C5. Moreover, the highest values of red fluorescence per cell were observed for NanoLowFLR and NanoHighFLR in C4, C5 and C6. Finally, larger cell size was recorded in C4, C5 and C6 than in C1, C2 and C3 for PicoLowFLR, Coccolithophore-like cells, NanoLowFLR and NanoHighFLR, but no pairwise assemblage was significantly different. The log-log relation between red fluorescence and orange fluorescence, per cell, showed an increase in fluorescence emission with the cell size (Fig. 9B). In addition, there was an increase in the red and orange fluorescence emission as the cell size increases (Fig. 9D) despite the standard deviation showed large variation for the orange fluorescence.

For red fluorescence, three orders of magnitude were recorded from the smallest (*Synechococcus*-like cells) to microphytoplankton cell size. *Synechococcus*-like and Cryptophyte-like cells could be characterized by a higher orange over red ratio from the other groups. However, not all groups subscribed to this relation. Indeed, the figure 10B showed that some groups exhibited a change in size but not in red fluorescence per cell (range of the standard deviations). This occur in specific communities or in each community. For example, PicoHighFLR exhibited a large range of cell size and red fluorescence in C6 and C1 whereas the size and the red fluorescence were fluctuating irrespective to each other in the rest of the communities. Such patterns were also observed for the Coccolithophore-like cells. This relation would mean that in some case the red fluorescence per cell is independent of the size of the cells. As chlorophyll *a* fluorescence reflects the endogenous concentration of this pigment, the relation between red fluorescence per cell and cell size may result

different intracellular pigment composition (Álvarez et al., 2017). On the other hand, the other groups (*i.e. Synechococcus*-like cells, PicoLowFLR, nanoeukaryotes, microphytoplankton and Cryptophyte-like cells) tended to show a balance between the size and the red fluorescence, the larger a cell was, the more red fluorescence it would emit. Finally, the range of the standard deviation in red and/or orange fluorescence emission showed that the emission of red fluorescence per cell within PicoLowFLR, PicoHighFLR, NanoLowFLR, NanoHighFLR, Cryptophyte-like cells and Coccolithophore-like cells groups were not proportional to the emission of orange fluorescence per cell. On the contrary, the emission of red fluorescence per cell was proportional to the emission of orange fluorescence per cell concerning *Synechococcus*-like cells and Microphytoplankton (Fig. 9D).

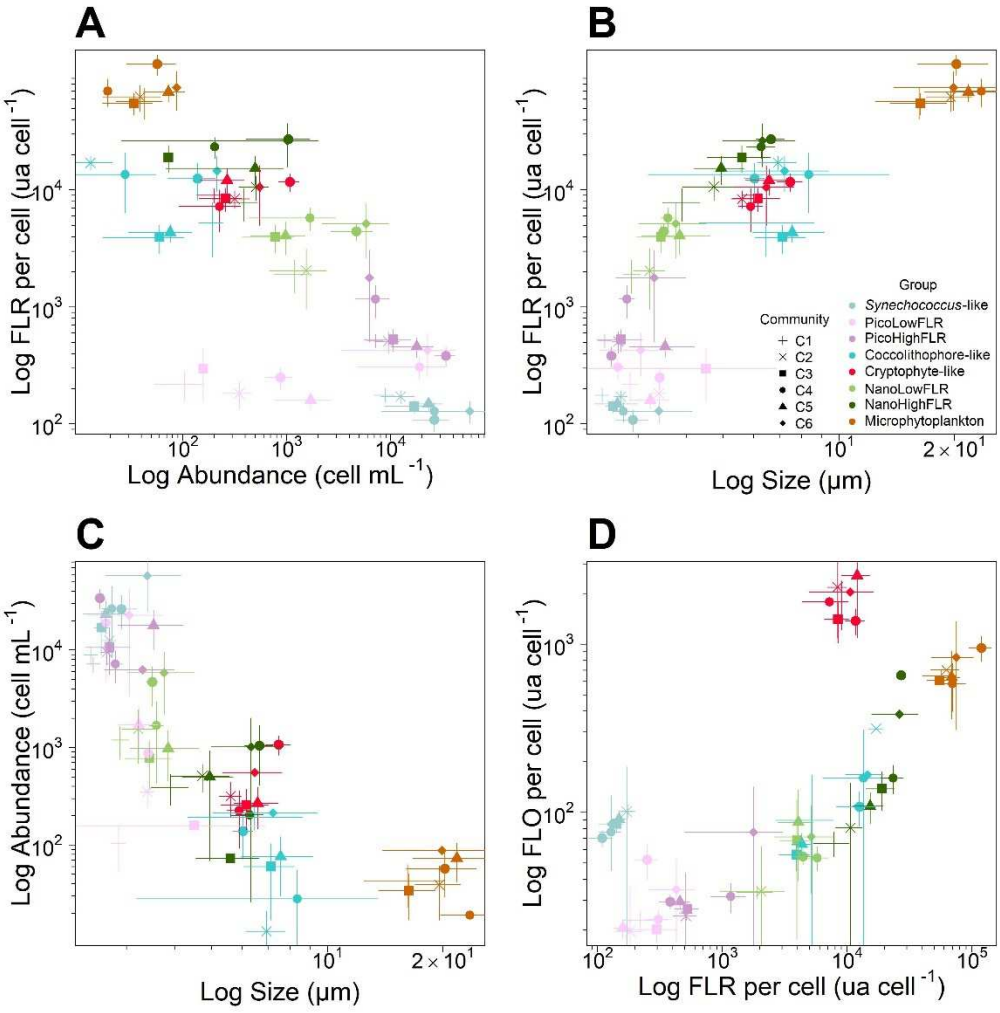

Figure 9: Patterns in size structure and fluorescence of phytoplankton groups amongst different communities defined in the English Channel. A. Log-log relationship between phytoplankton

abundance and the red fluorescence per cell, per group and per community, B. Log-log relationship of the red fluorescence per cell (FLR) against the phytoplankton size scaling per group and per community, C. Log-log relationship between phytoplankton cell size and abundance per group and per community, D. Log-log relationship of the orange fluorescence per cell (FLO) against the red fluorescence per cell (FLR) per phytoplankton group and per community.

3.4 Variance partitioning

Results of the variance partitioning (pure spatial, pure environmental, interaction between environment and space and unexplained variance) of the whole phytoplankton community and of each of the six assemblages were summarized in table 2. Such analysis revealed that spatial (PCNM spatial descriptors) and environmental variables (temperature, salinity and turbidity) accounted for 65% of the total variance on the whole cruise. The 35% of the residual variance (*i.e.* unexplained variance) were explained by other factors than environmental variables and space (*e.g.* biological processes such as grazing, infection without interaction with the environmental data; Table 2). The spatial descriptors (based on the spatial coordinates of sampling points) were more important than the environmental variables (<5% for all the groups) in structuring the abundance and total red fluorescence of each group. The spatial descriptors ranged between 24% (Coccolithophore-like cells) and 34%-36% (all the other groups). The results were provided in the supplementary table A.2. Focusing on the communities, the spatial variation of the assemblages was higher than the environmental variation within C1, C2, C3, C5 and C6. In community C4, the environmental variation accounted for 45% and was similar to the spatial variation which accounted for 43%. Then, the spatially structured environment (*i.e.* interaction) accounted between 13% (C1) and 46% (C6) of the total variation. Finally, considering the six communities identified (C5a and C5b are merged), both spatial and environmental variables accounted for a significant amount of variation except for the effect of the interaction between environment and space in C1. The sum of pure spatial, pure environmental variables and their interaction explained from 40% (C1) to 74% (C6) of the total variation in the communities. Therefore, the percentage of unexplained variation in the phytoplankton assemblages was comprised between 26% (C6) and 60% (C1).

Table 2: Variation partitioning of phytoplankton community (Environment including temperature, salinity and turbidity; space including abiotic interactions, physical processes and unexplained environment).

	Environment		Space		Interaction		Residual
	R^2 Adj.	p-value	R^2 Adj.	p-value	R^2 Adj.	p-value	
All	0.26	0.001	0.65	0.001	0.26	0.001	0.35
C1	0.15	0.001	0.25	0.001	0.13	0.06	0.60
C2	0.19	0.001	0.51	0.001	0.16	0.001	0.47
C3	0.59	0.001	0.60	0.001	0.43	0.001	0.34
C4	0.45	0.001	0.43	0.001	0.36	0.001	0.49
C5	0.35	0.001	0.44	0.001	0.27	0.001	0.48
C6	0.50	0.001	0.70	0.001	0.46	0.001	0.26

3.5 Scale of variability of phytoplankton communities

The multivariate Mantel correlogram based on the abundance and the average total red fluorescence per cluster revealed phytoplankton communities' spatial pattern by computing the geographical distance between pairs of sites in each community (Fig. 10). The Mantel correlogram indicated the highest autocorrelation at nearer distances, with a decrease and always reaching negative values at farther distances (but not always at the same distance). Because C5 community was not spatially continuous, C5 community was split into C5a (Eastern Bay of Seine) and C5b (South-Western of the WEC) sub-groups. The highest autocorrelation was found in C4 and C5b (r=0.34 and r=0.40, respectively). Phytoplankton assemblages showed a positive spatial autocorrelation between 20 km (C5a) and 110 km (C6, Fig. 11). This meant that phytoplankton composition became more different when the autocorrelation reached null or negative values. The definition of the spatial scale resulted in the combination of high correlation for the nearer distances and the quick decrease of the correlation when the distance increased. Here, the results suggested a high spatial structure at sub-mesoscale (<10 km) up to 110 km. This analysis confirmed the results of the partitioning variance analysis which mentioned that space had a great influence in structuring the assemblages.

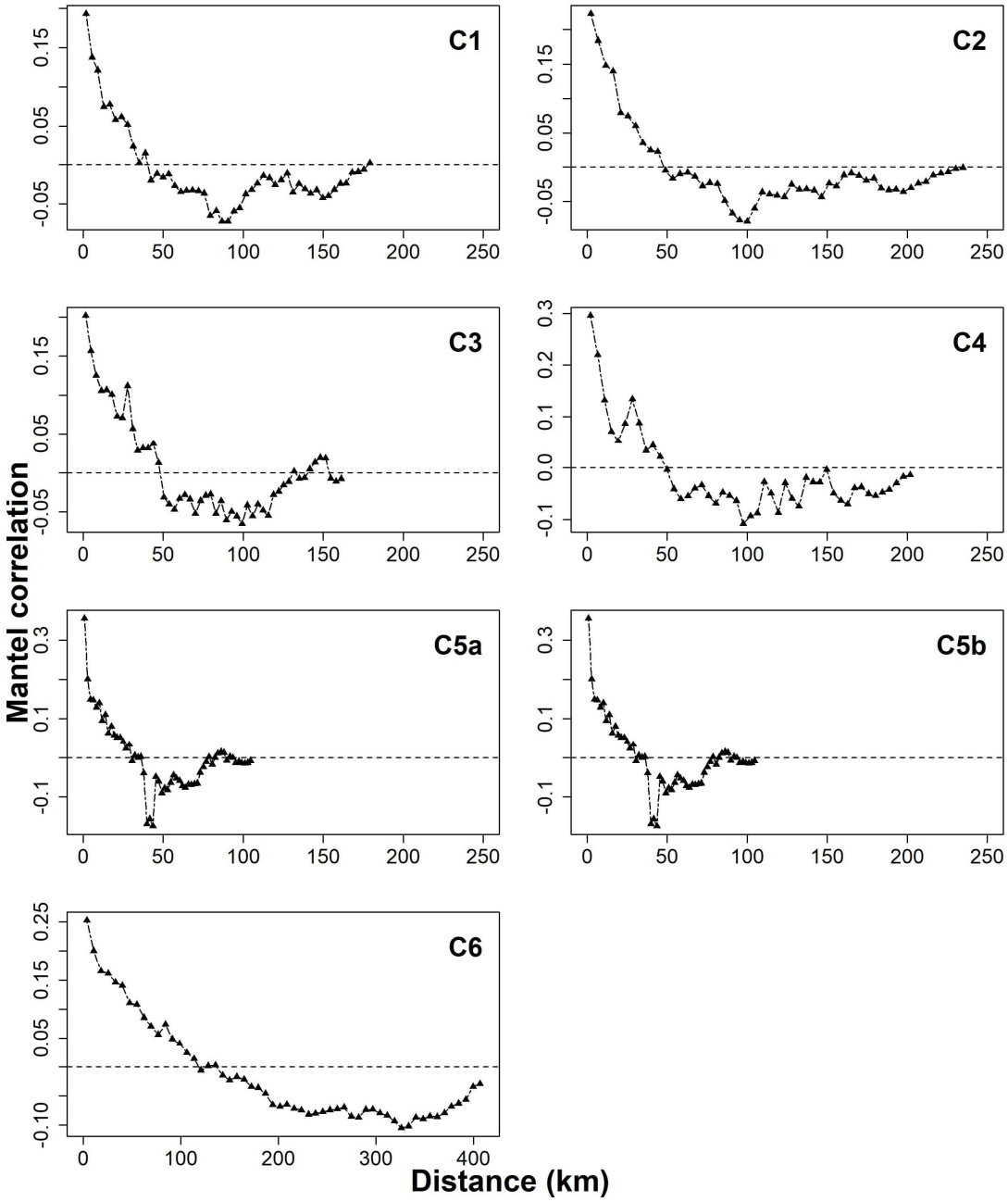

517

518 Figure 10: Mantel Correlogram of pairwise similarity in phytoplankton communities (Jaccardized
519 Czekanowski similarity based on the abundance and average total red fluorescence per cluster) against
520 geographical distance (Euclidean distance).

521

522 **4. Discussion**

523 **4.1 Water masses**

Despite the English Channel is a rather well-studied area, only few surveys attempted to characterise the spatiotemporal distribution of physicochemical parameters in the CEC and WEC (Bentley et al., 1999; Charria et al., 2016; Garcia-Soto and Pingree, 2009; Napoléon et al., 2014, 2012). Most studies benefited of long-term coastal monitoring or transect of ships-of-opportunity through a year. In the present study, the focus was put in the whole Western and Central English Channel gridded at a specific period of a year. Although the sampling strategies differed, our results showed similar hydrological areas than previous studies. The water circulation from West to East in the English Channel explained the longitudinal gradient observed during our study especially for the slow salinity decrease (Salomon and Breton, 1993). In addition to this circulation, the vertical stability induced during summer, contributed to the longitudinal gradient of temperature. Along the English coast of the Central English Channel, the high values of turbidity were congruent with continuous run-off from the Solent and were entertained in the gyre of the Southern part of the Isle of Wight (Ménesguen and Gohin, 2006). During the CAMANOC cruise, strong horizontal gradients of temperature, salinity and turbidity revealed five distinct water masses. The temperature gradient revealed tidal mixing fronts where a strong stratification occurred (Simpson and Nunes, 1981). The stratification of the Ushant frontal area (Garcia-Soto and Pingree, 2009; Pingree, 1980; Pingree et al., 1975; Pingree and Griffiths, 1978) separated 2 water masses (WM). WM3 corresponded to Western English Channel (WEC) waters displaying mixed water column, lower temperature and higher salinity than the rest of the waters of the outer Channel (shelf front) and the eastern WEC. WM3 was surrounded by stratified waters. The western boundary corresponded to an external front separating warm and stratified waters (Celtic Seas shelf waters) from mixed and cold waters (WM3). At the east, an internal front separated cold and mixed waters (WM3) from warm and well-mixed waters (WM1). The temperature pattern observed in the offshore waters was not consistent with observation in 2011 (Marrec et al., 2013; Napoléon et al., 2013) but was congruent with negative anomaly observed in 2012 in the northern part of the WEC (Marrec et al., 2014). We explained that by a combination of a relatively higher stability of water in WM3 (low tidal stream) than in the CEC (high tidal stream) and the lower temperature which are supported by air-sea heat fluxes shifting from positive to negative balance during the summer-autumn transition. Thus, the upper mixed layer deepens and water cools down (Hoch and

552 Garreau, 1998). WM1 was characterized by high stable temperature and salinity (Fig. 4B). It might
553 have corresponded to the external front separating the WEC and the Celtic Seas in the Western border
554 and the internal front between the WEC and the CEC in the Eastern border. A latitudinal salinity
555 gradient revealed a salinity front separating WM4 found in the Bay of Seine (BOS) from the CEC
556 waters (WM2). The turbidity gradient separated the offshore waters of the CEC from English coastal
557 waters of Central English Channel (WM5). The low values of N^2 in WM4 (BOS) resulted from
558 permanently mixed waters even under the influence of the run-off of the Seine River (Bay of Seine;
559 French coast) whereas WM5 might have been under the remote influence of the Solent (English
560 Coast), leading to a slight dilution of coastal waters (compared to lower salinities recorded in the Bay
561 of Seine). WM2 could result in intermittently stratified waters (Van Leeuwen et al., 2015) in the
562 continuity of WEC stratified waters.

563 **4.2 Phytoplankton communities**

564 Several studies attempted to numerate phytoplankton assemblages in the whole area of the WEC and
565 CEC but none of them with high spatial (Garcia-Soto and Pingree, 2009; Napoléon et al., 2014, 2013,
566 2012) expanded gridding of data or on high temporal resolution (Edwards et al., 2001). Furthermore,
567 in this area, while previous studies focused only on species of the large size fraction of the
568 phytoplankton (*i.e.* microphytoplankton; Napoléon et al., 2014, 2012; Smyth et al., 2010; Tarran and
569 Bruun, 2015; Widdicombe et al., 2010), we were able to detect the whole size-range of phytoplankton
570 from picophytoplankton (1 µm) to large microphytoplankton (several millimeters length) in a single
571 analysis. Even though we did not reach a taxonomical resolution, it was possible to address the fine
572 structure of phytoplankton functional groups, as well as some of their traits, during the summer-
573 autumn transition.

574 In this study, we used the CytoSense parameters derived from the optical features and signatures as
575 cytometric-derived traits at the individual and populational level (Violle et al., 2007) while several
576 studies were applying the same technique and approach in different aquatic ecosystems focusing only
577 one level (Fragoso et al., 2019; Malkassian et al., 2011; Pomati et al., 2011; Pomati and Nizzetto,
578 2013). The four selected traits (abundance per group, orange and red fluorescence per cell and cell

size) showed a spatial heterogeneity for each group, between the communities (Litchman et al., 2010). The cell size was independent of cell's physiology per group between our communities (larger cells and higher average red fluorescence per cell in the community of the WEC, C4 and C6 than in the communities of CEC and BOS, C1, C2, C3 and C5). This result suggests specific responses of the species and/or groups. Indeed, in order to explain the spatial heterogeneity of the traits, we propose three hypothesis: (i) the selection of the optimal traits under biological pressures such as grazing (Litchman et al., 2009); (ii) the plasticity and genetic adaptation of the traits derived from the gene expression in response to environmental variations (Litchman et al., 2010) and; (iii) in the case of the automated "pulse shape" flow cytometry, a group can pool several species with similar optical properties (Thyssen et al., 2008a). Here, as grazers were not recorded continuously, we decided not to discuss about this hypothesis but would rather investigate the two others.

First, we suggest that the main drivers of the spatial variations are the temperature and the vertical stability of water masses. The results showed that PicoLowFLR group, Cryptophyte-like cells, nanoeukaryotes and microphytoplankton of the communities characterizing stratified and warm waters (C4) and mixed and cold waters (C6) exhibited the largest average cells size and the highest red and orange fluorescence per cell. Because the optimum for growth range of both nanoeukaryotes and microphytoplankton is relatively low, the colder temperatures measured in WM3, characterized mainly by C6, might have contributed to enhance their metabolism, hence, their size (Marañón, 2015). On the contrary, despite small phytoplankton (picophytoplankton) are dominant everywhere at this period, their growth is facilitated in water masses exhibiting high temperature values (C1 to C5, all WM except WM3). Indeed, their temperature optimum for growth range is higher than nanophytoplankton and microphytoplankton optimum growth range and should favor them in those conditions. Thus, in water masses exhibiting cold water, we expect a dominance of larger cell size whereas in warmer waters a dominance of the smaller cell size within a group. Although, nutrient and grazing rate were not available at the same spatiotemporal resolution as the biological data, we are aware that both play a role on cell size as well as their physiology. In the first case, the growth of small cells (*i.e.* *Synechococcus*-like cells and picoeukaryotes) is favored against large cells (*i.e.* microphytoplankton) under low nutrient condition (usually from the end of the spring bloom to fall). Then, biological

interactions (grazing, parasitism) are usually to impact cell size (Bergquist et al., 1985; Marañón, 2015) and physiology (Litchman, 2007; Litchman et al., 2010; Litchman and Klausmeier, 2008). Finally, size overestimation of *Synechococcus*-like cells and picoeukaryote (Fig. 9) results of technical drawbacks of flow cytometry. It is attributed to the halo effect of the laser which increased as particle were increasingly smaller than the width of the laser beam (*i.e.* 5µm).

The heterogeneity of environmental conditions within a water mass affect the expression of the traits within each group. For example, the Coccolithophorids are known to prefer warm and stable waters (WM1) for their growth. Here, the PSFCM detected high total abundance of this group in the Celtic Seas shelf, out of the English Channel (WM1, Fig. 5 and 6) which are dominated in this range of abundance by *Emilinia huxleyi* (Garcia-soto et al., 1995). On the contrary, microphytoplankton (including some diatoms and dinoflagellates) are known to grow and exhibit higher size in cold waters, turbulent system, rich in nutrient. This explanation is also true for the nanoeukaryotes (*i.e.* NanoLowFLR and NanoHighFLR). This is congruent with the WM3 and WM4 being influenced by the Seine river (C5) and both by the Atlantic Ocean waters and the Seine River (C3). They both contribute to provide nutrients. In addition, the low vertical water stability observed in the coastal communities (along the French coast of Brittany, Bay of Seine) could increase small-scale turbulence which might be positive for some groups (microphytoplankton, Cryptophytes-like, nanoeukaryotes) by increasing nutrient transport (Karp-Boss et al., 1996).

On the other hand, all the groups exhibited different levels of red and orange fluorescence per cell between the communities, except *Synechococcus*-like cells which showed the same levels across the communities (Fig. 9A, B and D). The fluorescence emission given by each group is dependent on the physiological states of the cells. The quantum yield of the chlorophyll *a* fluorescence (*i.e.* red fluorescence of the PSFCM) and phycobilin and phycoerythrin (*i.e.* orange fluorescence of the PSFCM) is also dependent to the life cycle of the cells leading to high fluorescence for young and efficient cells whereas lysis is decreasing the fluorescence emission. Another point was linked to the atmospheric conditions during the cruise. At the beginning of the cruise (corresponding mainly to communities C6, C5 and C4 in WEC waters), the weather was sunny and without wind, some groups (picoeukaryotes, nanoeukaryotes and microphytoplankton) showed high variability in orange

fluorescence per cell within a single community. The strong light intensity and the high stability might have resulted in the synthesis of photoprotective pigments. However, the change of weather after half of the cruise (while investigating WM3 and C1) might have enhanced the vertical mixing. Therefore, the position of phytoplankton cells of the groups is permanently engendered by the mixing of the water column which do not the induce production of photoprotective pigments.

Finally, the last case concerns the lack of taxonomical resolution of the automated "pulse shape-recording" flow cytometer. Indeed, our number of groups was limited. By sharing similar optical properties, several species are attributed to a same cluster. In WEC waters, flow cytometry surveys showed that picophytoplankton is usually composed of Prasinophyceae and usually dominated by *Ostreococcus sp.* at this period of the year (which are considered as red picoeucaryotes by flow cytometry). In addition, among the cryptophytes, few genera exhibiting a wide size range (between 5 and 19µm) are commonly detected (Marie et al., 2010). Nanoeukaryotes are frequently represented by Haptophytes, Stramenopiles and Chlorophytes. *Emiliania huxleyi* is always reported as the dominant coccolithophore species and is known to bloom in the outer shelf of the WEC (Garcia-soto et al., 1995). In addition, a high diversity of diatoms and dinoflagellates is also observed in the WEC (*e.g.* Widdicombe et al., 2010). Such taxonomical diversity results also in size diversity which is related to physiological traits (Litchman et al., 2010). Consequently, the pigment expression varies. Here, the variations of the trait's expression considering the three hypotheses (the plasticity and genetic adaptation of the traits, the selection of the optimal traits under biological pressures and the lack of taxonomical determination by automated "pulse shape-recording" flow cytometry) lead to changes in related traits such as nutrient uptake, cell carbon and nitrogen content within each groups and between the communities. The fact that traits such as the cell-size, abundance and total or per cell red fluorescence per group differed significantly between communities, suggests optimum growth conditions in the recorded abiotic parameters for their growth combined with trade-off in biological pressure and variations of the taxonomical composition.

4.3 Environment vs. spatial variations

We expected a greater influence of environment over space structuring phytoplankton communities in the English Channel. Indeed, abiotic filtering has been shown to play a key-role in shaping phytoplankton assemblages (Cornwell and Ackerly, 2015). However, in the present study, variation partitioning showed that variability in each community depended more on spatial (25 to 70%) than on environmental (15% to 59%) variation within space inducing significantly the environmental variations (16% to 46%; Table 2). Despite heterogeneity is well reported in other areas and seas (Bonato et al., 2015; Marrec et al., 2018; Thyssen et al., 2015), our study allowed quantifying the importance of space and environment on high frequency flow cytometry. Here, the spatiotemporal study of the phytoplankton communities showed an imbalance between groups over one location, this means that high abundance of a group coincided with low abundance of another group and vice-versa. For example, the highest abundance of Coccolithophore-like cells was observed out of the English Channel, in the Celtic Seas shelf where none of the other groups (except *Synechococcus*-like cells) exhibited highest abundance (Fig. 5). This was observed also for both picoeukaryote groups, the highest abundance of the PicoLowFLR was found where PiocHighFLR abundance was relatively low and vice-versa. NanoLowFLR and NanoHighFLR showed the same trend. As previously shown with temperature and vertical stability, each group might result of the selection by a combination of the best conditions (environmental, physical and biotic interactions) for their growth, metabolism and access to resources thus defining their ecological niche (Margalef, 1978; Reynolds, 2006, 1994, 1984; Tilman et al., 1982). Despite *Synechococcus*-like cells share the same environmental niche as picoeukaryotes (Chen et al., 2011), we could identify some spot of exclusion on both sides near the Ushant front between *Synechococcus*-like cells and PicoLowFLR and others between *Synechococcus*-like cells and PicoHighFLR which are consistent either with sharing niche (Chen et al., 2011) either with exclusions (Winder, 2009). However, both studies considered only one picoeukaryotes group and analyzed discrete samples while we could characterize at a high spatial and/or temporal resolution two sub-groups in the picoeukaryotes and *Synechococcus*-like cells. Consequently, the characterization of sub-groups may increase the ecological understanding of plankton functional groups. As previously discussed, phytoplankton traits are also known to partition ecological niche of species or functional groups (Litchman et al., 2010; Litchman and Klausmeier, 2008). Therefore, by extension, cytometry-

derived traits (Fragoso et al., 2019; Malkassian et al., 2011; Pomati et al., 2011; Pomati and Nizzetto, 2013) are important to be taken into account when considering the spatial and/or temporal ecological niche of the functional groups.

4.4 Spatial structure analysis

Based on the Mantel correlograms (Fig. 10), phytoplankton communities are autocorrelated from small to large scale (20 km to 110 km), depending on the communities. The highest correlation at nearer distance followed by the decrease in autocorrelation define a stronger structure for closer sampled units. Due to the high spatial resolution between two sampling units (*i.e.* 3.4 km), we state phytoplankton communities to be structured at the sub-mesoscale (1 – 10 km). The local structuration is also supported by the maps of each phytoplankton group (Fig. 5), their distribution with respect to the Ushant front (Fig. 6) and the coefficient of variation (Table 2), which highlighted heterogeneity and sharp shifts of total abundance, confirming a local structuration. This measure on the field was congruent with previous findings using conventional flow cytometry (Martin et al., 2005), remote sensing (d'Ovidio et al., 2010) and modelling (Lévy et al., 2014; Mahadevan et al., 2012). The positive autocorrelation found for each community reflects the size of the patches for communities. Several physical processes are well reported to generate patchiness. Small scale turbulence are well-known to generate patchiness which can concentrate particles and phytoplankton at very small scales (Schmitt and Seuront, 2008). Indeed, Pingree (Pingree, 1980; Pingree and Griffiths, 1978) noticed that the English Channel is characterised by small turbulent and persistent eddies. Because phytoplankton moves passively due to the movements of the fluids, eddies can generate patchiness of phytoplankton and spatial heterogeneity. This is commonly observed in the North Atlantic Ocean in the Western English Channel and the Bay of Seine (Mahadevan et al., 2012; Ménesguen and Gohin, 2006; Pingree et al., 1978; Salomon and Breton, 1993) as in our study, despite we could not observe the eddies. In the meanwhile, eddies contribute locally to water masses motion, changing the abiotic conditions which allow a niche specialization (d'Ovidio et al., 2010). The association of the front in the Western English Channel and the eddies frequently reported in the area are described to generate sub-mesoscale turbulence (*i.e.* 1 – 10 km; Bracco et al., 2000; Perruche et al., 2011). This latter and the

passive transport of phytoplankton cause the important dispersal rates of phytoplankton (Lévy et al., 2014). In our study, figure 4D defined the position of the fronts during the cruise and the figure 6 showed the distribution of each cytometric group with respect to the inner front. The dispersal rates reflected here the heterogeneity in abundance around the front. Moreover, the English Channel is highly hydrodynamical, exhibiting a heterogeneity between French and English coasts, Bay of Seine and offshore waters in the strength of the tidal stream. This component also induces the strength of the dispersal rate. Finally, high variability in each group's traits, inside each community, may also result in the spatial variation of the strength of the dispersal, which increased the plasticity (Sultan and Spencer, 2002; Via and Lande, 1985) thus the variability of their traits (Litchman et al., 2010).

5. Conclusion

In the present study, six phytoplankton communities were characterised based on the contribution of each of the eight defined cytometric groups and their optical features and signatures, total abundance and chlorophyll content. These optical features can be, to some extent, associated to life traits, from coastal to offshore waters, where long term regular monitoring does not exist. Phytoplankton and their derived traits were strongly dependent on the hydrology but, most of the times, the communities were even more structured by the spatial descriptors. They include parameters which are not taken into account in the environmental part such as positive and negative biological interactions, other unmeasured environmental parameters, physical processes. Mantel correlogram made possible to identify phytoplankton communities' variations at the sub-mesoscale (1 – 10 km) in the English Channel. Physical parameters were proposed to explain these variabilities, by structuring the hydrology (different water masses) as well as phytoplankton communities, which were not always associated to a single water mass. Further work should investigate the traits responses to the environmental conditions by applying high frequency flow cytometry in a regular basis, if possible, connected to automated hydrological and biogeochemical measurements at high frequency, on a seasonal and interannual basis. We could therefore define an extended phytoplankton typology within the English Channel including all size classes and also their corresponding traits. This work requires analysing data from the three tables (species or functional groups, environment and traits) and have

743 already been proposed for automated flow cytometry in previous studies (Breton et al., 2017; Fragoso
744 et al., 2019; Pomati et al., 2013) and should be generalized from individuals to the community level.

745 **Acknowledgments**

746 This work was carried out in the frame of the M.Sc. FOGEM (Université du Littoral-Côte d'Opale and
747 Université of Lille) internship co-funded by the Laboratory of Oceanology and Geosciences and the
748 "Pôle Environnement, Milieux Littoraux et Marins" of ULCO. At present Arnaud Louchart benefits of
749 a PhD grant of the Université du Littoral-Côte d'Opale and the French Region « Hauts-de-France ».
750 The CAMANOC cruise was funded by the DFF project. We would like to thank Morgane Travers, P.I.
751 of the CAMANOC cruise, the scientists involved, as well as the Captain and the crew of the R/V
752 Thalassa (IFREMER).

753 **References**

754 Alpine, A.E., Cloern, J.E., 1988. Phytoplankton growth rates in a light-limited environment, San
755 Francisco Bay. Mar. Ecol. Prog. Ser. 44, 167–173.

756 Álvarez, E., Nogueira, E., López-Urrutia, Á., 2017. In Vivo Single-Cell Fluorescence and Size
757 Scaling of Phytoplankton Chlorophyll Content . Appl. Environ. Microbiol. 83, 1–16.
758 https://doi.org/10.1128/aem.03317-16

759 Bentley, D., Hart, V., Guary, J.C., Statham, P.J., 1999. Dissolved nutrient distributions in the Central
760 English Channel. Cont. Shelf Res. 19. https://doi.org/10.1016/S0278-4343(99)00054-0

761 Bergquist, A.M., Carpenter, S.R., Latino, J.C., 1985. Shifts in phytoplankton size structure and
762 community composition during grazing by contrasting zooplankton assemblages. Limnol.
763 Oceanogr. 30, 1037–1045.

764 Bonato, S., Breton, E., Didry, M., Lizon, F., Cornille, V., Lécuyer, E., Christaki, U., Artigas, L.F.,
765 2016. Spatio-temporal patterns in phytoplankton assemblages in inshore-offshore gradients using
766 flow cytometry: A case study in the eastern English Channel. J. Mar. Syst. 156, 76–85.
767 https://doi.org/10.1016/j.jmarsys.2015.11.009

768 Bonato, S., Christaki, U., Lefebvre, A., Lizon, F., Thyssen, M., Artigas, L.F., 2015. High spatial
769 variability of phytoplankton assessed by flow cytometry, in a dynamic productive coastal area, in
770 spring: The eastern English Channel. Estuar. Coast. Shelf Sci. 154, 214–223.
771 https://doi.org/10.1016/j.ecss.2014.12.037

772 Borcard, D., Legendre, P., 2002. All-scale spatial analysis of ecological data by means of principal
773 coordinates of neighbour matrices. Ecol. Modell. 153, 51–68.
774 https://doi.org/10.1016/j.catena.2016.01.006

775 Bracco, A., Provenzale, A., Scheuring, I., 2000. Mesoscale vortices and the paradox of the plankton.
776 Proc. R. Soc. B Biol. Sci. 267, 1795–1800. https://doi.org/10.1002/lipi.19660680811

777 Breton, E., Christaki, U., Bonato, S., Didry, M., Artigas, L.F., 2017. Functional trait variation and

778 nitrogen use efficiency in temperate coastal phytoplankton. Mar. Ecol. Prog. Ser. 563, 35–49.
779 https://doi.org/10.3354/meps11974

780 Brylinski, J.M., Lagadeuc, Y., 1990. L'interface eaux côtières/eaux du large dans le Pas-de-Calais
781 (côte française) : une zone frontale. Comptes rendus l'Académie des Sci. 311, 535–540.

782 Charria, G., Lamouroux, J., De Mey, P., 2016. Optimizing observational networks combining gliders,
783 moored buoys and FerryBox in the Bay of Biscay and English Channel. J. Mar. Syst. 162, 112–
784 125. https://doi.org/10.1016/j.jmarsys.2016.04.003

785 Chen, B., Wang, L., Song, S., Huang, B., Sun, J., Liu, H., 2011. Comparisons of picophytoplankton
786 abundance, size, and fluorescence between summer and winter in northern South China Sea.
787 Cont. Shelf Res. 31, 1527–1540. https://doi.org/10.1016/j.csr.2011.06.018

788 Collier, J.L., 2000. Flow cytometry and the single cell in phycology. J. Phycol. 36, 628–644.
789 https://doi.org/10.1046/j.1529-8817.2000.99215.x

790 Cornwell, W.K., Ackerly, D.D., 2015. Community Assembly and Shifts in Plant Trait Distributions
791 across an Environmental Gradient in Coastal California Published by : Ecological Society of
792 America Community across an environmental in plant trait distributions assembly and shifts
793 gradient and. Ecol. Monogr. 79, 109–126. https://doi.org/10.1890/07-1134.1

794 Cullen, J., Ciotti, A., Davis, R., Lewis, M., 1997. Emerging technologies and modeling. Limnol.
795 Oceanogr. 42, 1223–1239.

796 d'Ovidio, F., De Monte, S., Alvain, S., Dandonneau, Y., Levy, M., 2010. Fluid dynamical niches of
797 phytoplankton types. Proc. Natl. Acad. Sci. 107, 18366–18370.
798 https://doi.org/10.1073/pnas.1004620107

799 De Monte, S., Soccodato, A., Alvain, S., D'Ovidio, F., 2013. Can we detect oceanic biodiversity
800 hotspots from space? ISME J. 7, 2054–2056. https://doi.org/10.1038/ismej.2013.72

801 Dubelaar, G.B.J., Geerders, P.J.F., Jonker, R.R., 2004. High frequency monitoring reveals
802 phytoplankton dynamics. J. Environ. Monit. 6, 946–952. https://doi.org/10.1039/b409350j

803 Dubelaar, G.B.J., Gerritzen, P.L., Beeker, A.E.R., Jonker, R.R., Tangen, K., 1999. Design and first
804 results of CytoBuoy: A wireless flow cytometer for in situ analysis of marine and fresh waters.
805 Cytometry 37, 247–254.

806 Edwards, M., Reid, P., Planque, B., 2001. Long-term and regional variability of phytoplankton
807 biomass in the Northeast Atlantic (1960-1995). ICES J. Mar. Sci. 58, 39–49.
808 https://doi.org/10.1006/jmsc.2000.0987

809 Eloire, D., Somerfield, P.J., Conway, D.V.P., Halsband-Lenk, C., Harris, R., Bonnet, D., 2010.
810 Temporal variability and community composition of zooplankton at station L4 in the Western
811 Channel: 20 years of sampling. J. Plankton Res. 32, 657–679.
812 https://doi.org/10.1093/plankt/fbq009

813 Falkowski, P.G., 1994. The role of phytoplankton photosynthesis in global biogeochemical cycles.
814 Photosynth. Res. 39, 235–258. https://doi.org/10.1007/BF00014586

815 Falkowski, P.G., Barber, R.T., Smetacek, V., 1998. Biogeochemical Controls and Feedbacks on Ocean
816 Primary Production. Science (80-.). 281, 200–206. https://doi.org/10.1126/science.281.5374.200

817 Falkowski, P.G., Laws, E.A., Barber, R.T., Murray, J.W., 2003. Phytoplankton and Their Role in
818 Primary, New, and Export Production, in: Ocean Biogeochemistry. pp. 99–121.
819 https://doi.org/10.1007/978-3-642-55844-3_5

820 Field, C.B., Behrenfeld, M.J., Randerson, J.T., Falkowski, P., 1998. Primary production of the
821 biosphere: Integrating terrestrial and oceanic components. Science (80-.). 281, 237–240.
822 https://doi.org/10.1126/science.281.5374.237

823 Foulon, E., Not, F., Jalabert, F., Cariou, T., Massana, R., Simon, N., 2008. Ecological niche
824 partitioning in the picoplanktonic green alga Micromonas pusilla: Evidence from environmental
825 surveys using phylogenetic probes. Environ. Microbiol. 10, 2433–2443.
826 https://doi.org/10.1111/j.1462-2920.2008.01673.x

827 Fragoso, G.M., Poulton, A.J., Pratt, N., Johnsen, G., Purdie, D.A., 2019. Trait-based analysis of
828 subpolar North Atlantic phytoplankton and plastidic ciliate communities using automated flow
829 cytometer. Limnol. Oceanogr. 64, 1–16. https://doi.org/10.1002/lno.11189

830 Garcia-soto, C., Fernández, E., Pingree, R.D., Harbour, D.S., 1995. Evolution and structure of a shelf
831 coccolithophore bloom in the western English channel. J. Plankton Res. 17, 2011–2036.
832 https://doi.org/10.1093/plankt/17.11.2011

833 Garcia-Soto, C., Pingree, R.D., 2009. Spring and summer blooms of phytoplankton
834 (SeaWiFS/MODIS) along a ferry line in the Bay of Biscay and western English Channel. Cont.
835 Shelf Res. 29, 1111–1122. https://doi.org/10.1016/j.csr.2008.12.012

836 Goberville, E., Beaugrand, G., Sautour, B., Tréguer, P., 2010. Climate-driven changes in coastal
837 marine systems of western Europe. Mar. Ecol. Prog. Ser. 408, 129–147.
838 https://doi.org/10.3354/meps08564

839 Gregg, W.W., Conkright, M.E., Ginoux, P., O'Reilly, J.E., Casey, N.W., 2003. Ocean primary
840 production and climate: Global decadal changes. Geophys. Res. Lett. 30, 10–13.
841 https://doi.org/10.1029/2003GL016889

842 Haraguchi, L., Jakobsen, H.H., Lundholm, N., Carstensen, J., 2017. Monitoring natural phytoplankton
843 communities: A comparison between traditional methods and pulse-shape recording flow
844 cytometry. Aquat. Microb. Ecol. 80, 77–92. https://doi.org/10.3354/ame01842

845 Hoch, T., Garreau, P., 1998. Phytoplankton dynamics in the english channel: A simplified three-
846 dimensional approach. J. Mar. Syst. 16, 133–150. https://doi.org/10.1016/S0924-7963(97)00103-
847 6

848 Holligan, P.M., Harbour, D.S., 1977. The vertical distribution and succession of phytoplankton in the
849 mwestern english channel in 1975 and 1976. J. Mar. Biol. Assoc. United Kingdom 57, 1075–
850 1093. https://doi.org/10.1017/S002531540002614X

851 Hydes, D.J., Wright, P.N., 1999. SONUS: The southern nutrients study 1995-1997. Rep. Southampt.
852 Oceanogr. Cent.

853 Iriarte, A., Purdie, D.A., 2004. Factors controlling the timing of major spring bloom events in an UK
854 south coast estuary. Estuar. Coast. Shelf Sci. 61, 679–690.
855 https://doi.org/10.1016/j.ecss.2004.08.002

856 Jouenne, F., Lefebvre, S., Véron, B., Lagadeuc, Y., 2007. Phytoplankton community structure and
857 primary production in small intertidal estuarine-bay ecosystem (eastern English Channel,
858 France). Mar. Biol. 151, 805–825. https://doi.org/10.1007/s00227-006-0440-z

859 Karp-Boss, L., Boss, E., Jumars P.A, 1996. Nutrient Fluxes to Planktonic Osmotrophs in the Presence
860 of Fluid Motion. Oceanogr. Mar. Biol. an Annu. Rev. 34, 71–107.

861 Kifle, D., Purdie, D.A., 1993. The seasonal abundance of the phototrophic ciliate Mesodinium rubrum
862 in Southemptom water, England. J. Plankton Res. 5, 823–833.

Lampert, W., Fleckner, W., Rai, H., Taylor, B.E., 1986. Phytoplankton control by grazing zooplankton: A study on the spring clear□water phase. Limnol. Oceanogr. 31, 478–490. https://doi.org/10.4319/lo.1986.31.3.0478

Landeira, J.M., Ferron, B., Lunven, M., Morin, P., Marie, L., Sourisseau, M., 2014. Biophysical interactions control the size and abundance of large phytoplankton chains at the ushant tidal front. PLoS One 9, e90507. https://doi.org/10.1371/journal.pone.0090507

Leakey, R.J.G., Burkill, P.H., Sleigh, M.A., 1992. Planktonic ciliates in Southampton Water: abundance, biomass, production, and role in pelagic carbon flow. Mar. Biol. 114, 67–83. https://doi.org/10.1038/470444a

Lefebvre, A., Poisson-Caillault, E., 2019. High resolution overview of phytoplankton spectral groups and hydrological conditions in the eastern English Channel using unsupervised clustering. Mar. Ecol. Prog. Ser. 608, 73–92. https://doi.org/https://doi.org/10.3354/meps12781

Legendre, P., Legendre, L., 1998. Numerical ecology. 2nd. Elsevier Sci. https://doi.org/10.1017/CBO9781107415324.004

Lévy, M., Jahn, O., Dutkiewicz, S., Follows, M.J., 2014. Phytoplankton diversity and community structure affected by oceanic dispersal and mesoscale turbulence. Limnol. Oceanogr. Fluids Environ. 4, 67–84. https://doi.org/10.1215/21573689-2768549

Litchman, E., 2007. Resource Competition and the Ecological Success of Phytoplankton, in: Falkowski, P.G., Knoll, A.H. (Eds.), Evolution of Primary Producers in the Sea. Academic Press, pp. 351–375. https://doi.org/https://doi.org/10.1016/B978-0-12-370518-1.X5000-0

Litchman, E., de Tezanos Pinto, P., Klausmeier, C.A., Thomas, M.K., Yoshiyama, K., 2010. Linking traits to species diversity and community structure in phytoplankton. Hydrobiologia 653, 15–28. https://doi.org/10.1007/s10750-010-0341-5

Litchman, E., Klausmeier, C.A., 2008. Trait-Based Community Ecology of Phytoplankton. Annu. Rev. Ecol. Syst. 39, 615–639. https://doi.org/10.1146/annurev.ecolsys.39.110707.173549

Litchman, E., Klausmeier, C.A., Schofield, O.M., Falkowski, P.G., 2007. The role of functional traits and trade-offs in structuring phytoplankton communities: Scaling from cellular to ecosystem level. Ecol. Lett. 10, 1170–1181. https://doi.org/10.1111/j.1461-0248.2007.01117.x

Litchman, E., Klausmeier, C.A., Yoshiyama, K., 2009. Contrasting size evolution in marine and freshwater diatoms. Proc. Natl. Acad. Sci. 106, 2665–2670. https://doi.org/10.1073/pnas.0810891106

Mahadevan, A., D'Asaro, E., Lee, C., Perry, M.J., 2012. Eddy-Driven Stratification Initiates North Atlantic Spring Phytoplankton Blooms. Science (80-.). 337, 54–58.

Malkassian, A., Nerini, D., Van Dijk, M.A., Thyssen, M., Mante, C., Gregori, G., 2011. Functional analysis and classification of phytoplankton based on data from an automated flow cytometer. Cytom. Part A 79 A, 263–275. https://doi.org/10.1002/cyto.a.21035

Marañón, E., 2015. Cell Size as a Key Determinant of Phytoplankton Metabolism and Community Structure. Ann. Rev. Mar. Sci. 7, 241–264. https://doi.org/10.1146/annurev-marine-010814-015955

Margalef, R., 1978. Life-forms of phytoplankton as survival alternative in an unstable environment. Oceanologica 1, 493–509.

Marie, D., Shi, X.L., Rigaut-Jalabert, F., Vaulot, D., 2010. Use of flow cytometric sorting to better assess the diversity of small photosynthetic eukaryotes in the English Channel. FEMS Microbiol.

Ecol. 72, 165–178. https://doi.org/10.1111/j.1574-6941.2010.00842.x

Marrec, P., Cariou, T., Collin, E., Durand, A., Latimier, M., Macé, E., Morin, P., Raimund, S., Vernet, M., Bozec, Y., 2013. Seasonal and latitudinal variability of the CO 2 system in the western English Channel based on Voluntary Observing Ship (VOS) measurements. Mar. Chem. 155, 29–41. https://doi.org/10.1016/j.marchem.2013.05.014

Marrec, P., Cariou, T., Latimier, M., Macé, E., Morin, P., Vernet, M., Bozec, Y., 2014. Spatio-temporal dynamics of biogeochemical processes and air – sea CO 2 fl uxes in the Western English Channel based on two years of FerryBox deployment. J. Mar. Syst. 140, 26–38. https://doi.org/10.1016/j.jmarsys.2014.05.010

Marrec, P., Doglioli, A.M., Grégori, G., Dugenne, M., Della Penna, A., Bhairy, N., Cariou, T., Hélias Nunige, S., Lahbib, S., Rougier, G., Wagener, T., Thyssen, M., 2018. Coupling physics and biogeochemistry thanks to high-resolution observations of the phytoplankton community structure in the northwestern Mediterranean Sea. Biogeosciences 15, 1579–1606. https://doi.org/10.5194/bg-15-1579-2018

Martin, A.P., Zubkov, M. V., Burkill, P.H., Holland, R.J., 2005. Extreme spatial variability in marine picoplankton and its consequences for interpreting Eulerian time-series. Biol. Lett. 1, 366–369. https://doi.org/10.1098/rsbl.2005.0316

Ménesguen, A., Gohin, F., 2006. Observation and modelling of natural retention structures in the English Channel. J. Mar. Syst. 63, 244–256. https://doi.org/10.1016/j.jmarsys.2006.05.004

Menesguen, A., Hoch, T., 1997. Modelling the biogeochemical cycles of elements limiting primary production in the English Channel. I. Role of thermohaline stratification. Mar. Ecol. Prog. Ser. 146, 173–188.

Millie, D.F., Schofield, O.M., Kirkpatrick, G.J., Johnsen, G., Tester, P.A., Vinyard, B.T., 1997. Detection of harmful algal blooms using photopigments and absorption signatures: A case study of the Florida red tide dinoflagellate, Gymnodinium breve. Limnol. Oceanogr. 42, 1240–1251.

Napoléon, C., Fiant, L., Raimbault, V., Claquin, P., 2013. Study of dynamics of phytoplankton and photosynthetic parameters using opportunity ships in the western English Channel. J. Mar. Syst. 128, 146–158. https://doi.org/10.1016/j.jmarsys.2013.04.019

Napoléon, C., Fiant, L., Raimbault, V., Riou, P., Claquin, P., 2014. Dynamics of phytoplankton diversity structure and primary productivity in the English Channel. Mar. Ecol. Prog. Ser. 505, 49–64. https://doi.org/10.3354/meps10772

Napoléon, C., Raimbault, V., Fiant, L., Riou, P., Lefebvre, S., Lampert, L., Claquin, P., 2012. Spatiotemporal dynamics of physicochemical and photosynthetic parameters in the central English Channel. J. Sea Res. 69, 43–52. https://doi.org/10.1016/j.seares.2012.01.005

Not, F., Latasa, M., Marie, D., Cariou, T., Vaulot, D., Simon, N., 2004. A Single Species, Micromonas pusilla (Prasinophyceae), Dominates the Eukaryotic Picoplankton in the Western English Channel. Appl. Environ. Microbiol. 70, 4064–4072. https://doi.org/10.1128/AEM.70.7.4064

Pannard, A., Claquin, P., Klein, C., Le Roy, B., Véron, B., 2008. Short-term variability of the phytoplankton community in coastal ecosystem in response to physical and chemical conditions ' changes. Estuar. Coast. Shelf Sci. 80, 212–224. https://doi.org/10.1016/j.ecss.2008.08.008

Pearl, H.W., Valdes-Weaver, L.M., Joyner, A.R., Winkelmann, V., 2007. Phytoplankton indicators of ecological change in the eutrophying Pamlico sound system, North Carolina. Ecol. Appl. 17, 88–101.

Perruche, C., Pondaven, P., Lapeyre, G., Rivière, P., Carton, X., 2011. Effects of surface quasi-

geostrophic turbulence on phytoplankton competition and coexistence. J. Mar. Res. 69, 105–135. https://doi.org/10.1357/002224011798147606

Pingree, R.D., 1980. Physical Oceanography of the Celtic Sea and English Channel. Elsevier Oceanogr. Ser. 24, 415–465. https://doi.org/10.1016/S0422-9894(08)71358-8

Pingree, R.D., Griffiths, D.K.G., 1978. Tidal Fronts on the Shelf Seas Around the British Isles Marine Biological Association of the United Kingdom, Plymouth, England. J. Geophys. Res. Ocean. 83, 4615–4622. https://doi.org/10.1029/JC083iC09p04615

Pingree, R.D., Holligan, P.M., Head, R.N., 1977. Survival of dinoflagellates blooms in the western English Channel. Nature 265, 266–269. https://doi.org/10.1038/266309a0

Pingree, R.D., Holligan, P.M., Mardell, G.T., 1979. Phytoplankton growth and cyclonic eddies. Nature 278, 245–247.

Pingree, R.D., Holligan, P.M., Mardell, G.T., 1978. The effects of vertical stability on phytoplankton distributions in the summer on the northwest European Shelf. Deep-Sea Res. 25, 1011–1028. https://doi.org/10.1016/0146-6291(78)90584-2

Pingree, R.D., Pugh, P.R., Holligan, P.M., Forster, G.R., 1975. Summer phytoplankton blooms and red tides along tidal fronts in the approaches to the English Channel. Nature 258, 672–677. https://doi.org/10.1038/253600a0

Pomati, F., Jokela, J., Simona, M., Veronesi, M., Ibelings, B.W., 2011. An automated platform for phytoplankton ecology and aquatic ecosystem monitoring. Environ. Sci. Technol. 45, 9658–9665. https://doi.org/10.1021/es201934n

Pomati, F., Kraft, N.J.B., Posch, T., Eugster, B., Jokela, J., Ibelings, B.W., 2013. Individual Cell Based Traits Obtained by Scanning Flow-Cytometry Show Selection by Biotic and Abiotic Environmental Factors during a Phytoplankton Spring Bloom. PLoS One 8. https://doi.org/10.1371/journal.pone.0071677

Pomati, F., Nizzetto, L., 2013. Assessing triclosan-induced ecological and trans-generational effects in natural phytoplankton communities: A trait-based field method. Ecotoxicology 22, 779–794. https://doi.org/10.1007/s10646-013-1068-7

Rantajärvi, E., Olsonen, R., Hällfors, S., Leppänen, J.M., Raateoja, M., 1998. Effect of sampling frequency on detection of natural variability in phytoplankton: Unattended high-frequency measurements on board ferries in the Baltic Sea. ICES J. Mar. Sci. 55, 697–704. https://doi.org/10.1006/jmsc.1998.0384

Rassoulzadegan, F., Laval-Peuto, M., Sheldon, R.W., 1988. Partitioning of the food ration of marine ciliates between pico- and nanoplankton. Hydrobiologia 159, 75–88. https://doi.org/10.1007/BF00007369

Reynolds, C.S., 2006. Ecology of Phytoplankton, Cambridge. ed. Cambridge.

Reynolds, C.S., 1994. The long, the short and the stalled: on the attributes of phytoplankton selected by physical mixing in lakes and rivers. Hydrobiologia 289, 9–21.

Reynolds, C.S., 1984. The ecology of freshwater phytoplankton. Cambridge University Press.

Ribalet, F., Marchetti, A., Hubbard, K.A., Brown, K., Durkin, C.A., Morales, R., Robert, M., Swalwell, J.E., Tortell, P.D., Armbrust, V.E., 2010. Unveiling a phytoplankton hotspot at a narrow boundary between coastal and offshore waters. Proc. Natl. Acad. Sci. 107, 16571–16576. https://doi.org/10.1073/pnas.1005638107

992 Richardson, T.L., Pinckney, J.L., 2004. Monitoring of the toxic dinoflagellate Karenia brevis using
993 gyroxanthin-based detection methods. J. Appl. Phycol. 16, 315–328.
994 https://doi.org/10.1023/B:JAPH.0000047788.31312.4f

995 Rutten, T.P.A., Sandee, B., Hofman, A.R.T., 2005. Phytoplankton monitoring by high performance
996 flow cytometry: A successful approach? Cytom. Part A 64, 16–26.
997 https://doi.org/10.1002/cyto.a.20106

998 Salomon, J., Breton, M., 1993. An atlas of long-term currents in the Channel. Oceanol. acta 16, 439–
999 448.

1000 Schmitt, F.G., Seuront, L., 2008. Intermittent turbulence and copepod dynamics: Increase in encounter
1001 rates through preferential concentration. J. Mar. Syst. 70, 263–272.
1002 https://doi.org/10.1016/j.jmarsys.2007.01.008

1003 Schubert, A., Telcs, A., 2014. A note on the Jaccardized Czekanowski similarity index. Scientometrics
1004 98, 1397–1399. https://doi.org/10.1007/s11192-013-1044-2

1005 Simpson, J.H., Nunes, R.A., 1981. The tidal intrusion front: An estuarine convergence zone. Estuar.
1006 Coast. Shelf Sci. 13. https://doi.org/10.1016/S0302-3524(81)80024-2

1007 Smyth, T.J., Fishwick, J.R., Al-Moosawi, L., Cummings, D.G., Harris, C., Kitidis, V., Rees, A.,
1008 Martinez-Vicente, V., Woodward, E.M.S., 2010. A broad spatio-temporal view of the Western
1009 English Channel observatory. J. Plankton Res. 32, 585–601.
1010 https://doi.org/10.1093/plankt/fbp128

1011 Sournia, A., Birrien, J.L., Douvillé, J.L., Klein, B., Viollier, M., 1987. A daily study of the diatom
1012 spring bloom at Roscoff (France) in 1985. I. The spring bloom within the annual cycle. Estuar.
1013 Coast. Shelf Sci. 25, 355–367. https://doi.org/10.1016/0272-7714(87)90078-3

1014 Sultan, S.E., Spencer, H.G., 2002. Metapopulation Structure Favors Plasticity over Local Adaptation.
1015 Am. Nat. 160, 271–283.

1016 Tarran, G.A., Bruun, J.T., 2015. Nanoplankton and picoplankton in the Western English Channel:
1017 Abundance and seasonality from 2007-2013. Prog. Oceanogr. 137, 446–455.
1018 https://doi.org/10.1016/j.pocean.2015.04.024

1019 Thorel, M., Claquin, P., Schapira, M., Le Gendre, R., Riou, P., Goux, D., Le Roy, B., Raimbault, V.,
1020 Deton-Cabanillas, A.F., Bazin, P., Kientz-Bouchart, V., Fauchot, J., 2017. Nutrient ratios
1021 influence variability in Pseudo-nitzschia species diversity and particulate domoic acid production
1022 in the Bay of Seine (France). Harmful Algae 68, 192–205.
1023 https://doi.org/10.1016/j.hal.2017.07.005

1024 Thyssen, M., Alvain, S., Lefèbvre, A., Dessailly, D., Rijkeboer, M., Guiselin, N., Creach, V., Artigas,
1025 L.F., 2015. High-resolution analysis of a North Sea phytoplankton community structure based on
1026 in situ flow cytometry observations and potential implication for remote sensing. Biogeosciences
1027 12, 4051–4066. https://doi.org/10.5194/bg-12-4051-2015

1028 Thyssen, M., Mathieu, D., Garcia, N., Denis, M., 2008a. Short-term variation of phytoplankton
1029 assemblages in Mediterranean coastal waters recorded with an automated submerged flow
1030 cytometer. J. Plankton Res. 30, 1027–1040. https://doi.org/10.1093/plankt/fbn054

1031 Thyssen, M., Tarran, G.A., Zubkov, M. V., Holland, R.J., Grégori, G., Burkill, P.H., Denis, M.,
1032 2008b. The emergence of automated high-frequency flow cytometry: Revealing temporal and
1033 spatial phytoplankton variability. J. Plankton Res. 30, 333–343.
1034 https://doi.org/10.1093/plankt/fbn005

1035 Tilman, D., Kilham, S.S., Kilham, P., 1982. Phytoplankton Community Ecology: The Role of

Limiting Nutrients. Annu. Rev. Ecol. Syst. 13, 349–372.

Travers-Trolet, M., Verin, Y., 2014. CAMANOC cruise, RV Thalassa. https://doi.org/10.17600/14001900

Van Leeuwen, S., Tett, P., Mills, D., van der Molen, J., 2015. Stratified and nonstratified areas in the North Sea: Long-term variability and biological an policy implications. J. Geophys. Res. Ocean. 120, 4670–4686. https://doi.org/10.1002/2014JC010485.Received

Via, S., Lande, R., 1985. Genotype-Environment Interaction and the Evolution of Phenotypic Plasticity. Evolution (N. Y). 39, 505–522. https://doi.org/10.2307/2408649

Violle, C., Navas, M.L., Vile, D., Kazakou, E., Fortunel, C., Hummel, I., Garnier, E., 2007. Let the concept of trait be functional! Oikos 116, 882–892. https://doi.org/10.1111/j.0030-1299.2007.15559.x

Ward, J.H.J., 1963. Hierarchical grouping to optimize and objective function. J. Am. Stat. Assoc. 58, 236–244. https://doi.org/10.1080/01621459.1963.10500845

Widdicombe, C.E., Eloire, D., Harbour, D., Harris, R.P., Somerfield, P.J., 2010. Long-term phytoplankton community dynamics in the Western English Channel. J. Plankton Res. 32, 643–655. https://doi.org/10.1093/plankt/fbp127

Winder, M., 2009. Photosynthetic picoplankton dynamics in Lake Tahoe: Temporal and spatial niche partitioning among prokaryotic and eukaryotic cells. J. Plankton Res. 31, 1307–1320. https://doi.org/10.1093/plankt/fbp074

Highlights of manuscript CSR_2019_156

Automated flow cytometry addresses phytoplankton community changes at high frequency

Eight cytometric groups are characterized from pico- to microphytoplankton size range

Variation in cytometry-derived traits can be characterized between communities

Frontal structures drive phytoplantkon spatial distribution at sub-mesoscale

Conflict of interest

The authors declare that they have no conflict of interest.